ELECTROCHEMICAL DETECTION OF INTERACTIONS BETWEEN DNA AND VARIOUS LIGANDS

A Thesis Submitted to the College of Graduate Studies and Research
in Partial Fulfillment of the Requirements for the
Degree of Master of Science
in the Department of Biochemistry
University of Saskatchewan, Saskatoon

by

Alina Muresan

Permission to Use

In presenting this thesis in partial fulfillment of the requirements for a postgraduate degree from the University of Saskatchewan, I agree that the libraries of this University may make it freely available for inspection. I further agree that permission for copying of this thesis in any manner, in whole or in part, for scholarly purposes may be granted by the professors who supervised my thesis work, or in their absence, by the Head of the Department of Biochemistry or the Dean of the College of Medicine. It is understood that any copying or publication or use of this thesis or parts thereof for financial gain shall not be allowed without my written permission. It is also understood that due recognition shall be given to me and to the University of Saskatchewan in any scholarly use which may be made of any materials in my thesis.

Requests for permission to copy or make other use of material in this thesis in whole or in part should be addressed to:

Head of the Department of Biochemistry
University of Saskatchewan
Saskatoon, Saskatchewan, S7N 5E5

Acknowledgements

To begin with, I want to thank my supervisor, Dr. Jeremy Lee, for his guidance and support. It was an enriching and wonderful experience to work with Jeremy and I would recommend him as a supervisor to anyone interested in doing a graduate degree in biochemistry. I wish him good luck in all of his future projects.

I would also like to thank Dave, my dear husband, who puts up with all my ups and downs and who shows me his love every day. I also want to thank my parents, my grandmother, and my parents-in-law. It is wonderful to have such supportive and loving parents.

Finally, I would like to thank all of my colleagues in the lab, particularly Grant Bare, Michael Dinsmore, and Todd Sutherland for their helpful and insightful advice. However, working in a lab is not only the actual lab work and I must also thank all the other colleagues in the Lee lab who made my time there so pleasant and worthwhile.

TABLE OF CONTENTS

List of Figures

List of Abbreviations

A	adenine
BSA	bovine serum albumin
C	cytosine
C_{DL}	double-layer capacitance
DNA	2`-deoxyribonucleic acid
dsDNA	double-stranded DNA
$E^{0`}$	formal potential of an electrode
EIS	electrochemical impedance spectroscopy
Fab	antigen binding fragment
G	guanine
IgG	immunoglobulin G
me-BSA	methylated bovine serum albumin
NZB	New Zealand Black
NZW	New Zealand White
R_{CT}	charge-transfer resistance
R_S	solution resistance
SAM	self-assembled monolayer
SLE	systemic lupus erythematosus
ssDNA	single-stranded DNA
T	thymine
TAE	Tris-acetate-ethylenediaminetetraacetic acid buffer
Tris	tris[hydroxymethyl]aminomethane
W	Warburg impedance
Z	impedance
Z_{im}	the imaginary component of impedance
Z_{re}	the real component of impedance

Abstract

Antibodies specific for DNA, with varying degrees of sequence specificity, are common in many autoimmune diseases including systemic lupus erythematosus. The presence of anti-DNA antibodies is a useful determinant in arriving at a prognosis in these conditions. Given the prevalence of these diseases in both the developing and developed world and the difficulty that often accompanies diagnosis of autoimmune diseases, it is desirable to have sensitive, rapid, and inexpensive diagnostic tools for these diseases. Because of the great sensitivity of electrochemical techniques and their potential utility in characterizing interactions between macromolecules, electrochemistry has great potential as a diagnostic tool for any disease involving antibodies. Anti-DNA antibodies are present in many autoimmune diseases, notably systemic lupus erythematosus. Since DNA is a stable and well-characterized antigen, an electrochemical-based assay is particularly useful for diagnosis of these diseases.

The impedance of a gold surface was measured in the presence and absence of single- and double-stranded DNA monolayers. The DNA monolayer was diluted with butanethiol in order to provide a surface with more accessible binding sites than an undiluted monolayer. The change in impedance of the DNA monolayer following exposure to various small molecules and macromolecules was assessed. The molecules used included polyamines that induce conformational changes in DNA, proteins which bind DNA specifically, proteins which bind DNA non-specifically, and proteins which do not bind DNA. The presence of a DNA monolayer, whether single- or double-stranded, increased the impedance of the gold surface and dilution of the monolayers by butanethiol decreased the impedance, as expected. When exposed to polyamines, the impedance of the DNA monolayer decreased further. This could be due to lowered charge repulsion, to DNA condensation, or to a combination of both. When methylated bovine serum albumin was exposed to the monolayer, there was an increase in impedance. Conversely, when bovine serum albumin was exposed to the monolayer, the impedance was only increased at very high concentrations of protein. The increase following exposure to high concentrations of bovine serum albumin was likely due to deposition of protein on to the monolayer. The specificity of these interactions was illustrated by experiments with the antibody Hed 10, which binds single-stranded but not double-stranded DNA. Exposure to Hed 10 only caused a significant change in impedance when exposed to monolayers of single-stranded DNA.

The decreased impedance of the DNA monolayer caused by the presence of polyamines is consistent with the known structural perturbations induced by these molecules as measured with other methods. Similarly, the increase in impedance caused by the presence of proteins which bind DNA is consistent with increased steric interference by the protein-DNA complex. The failure of proteins which do not bind DNA to affect the impedance of the monolayer indicated that the effects in the experiments with DNA-binding proteins were due to protein binding and not other factors. The specificity of the assay as demonstrated by the results of the experiments with Hed 10 suggest that impedance-based measurements may provide the basis for a reliable, sensitive, and inexpensive assay for detecting the presence of anti-DNA antibodies in the serum of autoimmune disease patients.

1.0 Introduction

A large portion of the intracellular functions of living creatures, from prokaryotes to plants to mammals, depend on a specific and controlled interaction between nucleic acids and proteins. The specificity and strength of these interactions are governed by the exact structure of the interacting molecule (Roeder, 2005). Many diseases, notably some cancers, are caused by mutations in the genome. These mutations can affect the nucleic acid that is bound in a protein-DNA interaction. Alternatively, the mutation can be in the gene coding for a protein which interacts with DNA. Either of these types of mutations can adversely affect interactions between protein and DNA, which in turn disrupts regulation of cellular functions and can allow the growth of tumours (Hartwell and Kastan, 1994). In addition to specific interactions with nucleic acids, many proteins bind in non-specific ways to nucleic acids and to other proteins (Fraenkel-Conrat and Olcott, 1945). Because of non-specific interactions, which often occur alongside specific reactions, useful techniques for measuring specific interactions between nucleic acids and proteins must be very sensitive.

One class of interactions between nucleic acids and proteins that is very important to many autoimmune diseases is the interaction between antibodies and DNA. In many autoimmune diseases, anti-DNA antibodies with varying degrees of sequence specificity are generated and the presence of these antibodies can be a useful diagnostic tool for physicians. The utility of these antibodies as a diagnostic tool creates a need for a way to quickly and accurately determine whether they are present in the blood of a patient. Since all antibodies of the same class are essentially identical in terms of molecular mass, a useful way to assay for the presence of these particular antibodies would be on the basis of their specificity for different DNA sequences (Swanson *et al.*, 1996). Electrochemical techniques can provide a variety of different types of data about binding events on a surface (Bard and Faulkner 2001). Thus, electrochemical techniques may be a useful starting point for developing accurate assays to detect for the presence of anti-DNA antibodies in the serum of autoimmune disease patients.

1.1 Electrochemistry

1.1.1 Electrochemical Impedance Spectroscopy

One of the primary systems studied in biochemistry is the interaction between nucleic acids and proteins. Many different biochemical and biophysical methods are used to characterize these interactions. An emerging electrochemical technique in such studies is electrochemical impedance spectroscopy (EIS). In EIS studies, three electrodes are employed to conduct an experiment: the working, reference, and counter electrodes (Li *et al.*, 2003). These three electrodes are placed in a glass container filled with a solution of redox probe, all of which together are referred to as an electrochemical cell. An electrochemical cell is illustrated in figure 1.

The working electrode typically has a gold surface at one end; the rest of it is usually constructed of an inert material. The working electrode is the surface on which the reactions of interest take place and in EIS studies on nucleic acids it would typically have a 2`-deoxyribonucleic acid (DNA) monolayer covalently immobilized to the gold surface via S-Au bonds. The reference electrode is typically a piece of silver wire coated with AgCl and contained within a glass tube filled with a 3 M NaCl solution saturated with AgCl. The reference electrode is always at a known potential; this fixed value provides a standard against which to measure the working electrode potential. The counter electrode is typically a platinum wire that allows the current to flow in the solution between the working and the counter electrode. The electrochemical cell is in turn connected to a potentiostat. A potentiostat is an instrument that controls the potential of the working electrode and measures the resulting current. During an EIS experiment, impedance is measured as a function of the frequency of the AC source, which is varied. EIS is very sensitive and is capable of probing multiple charge transfer parameters of a system (Bard and Faulkner 2001). The individual components of impedance that can be differentiated and investigated using EIS are discussed below in section 1.1.3.

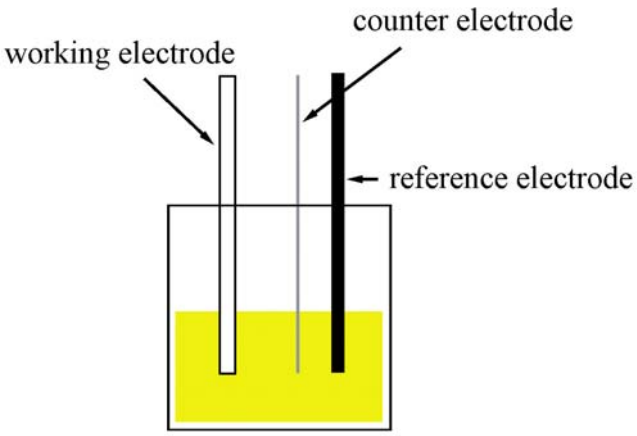

Figure 1: An illustration of an electrochemical cell, showing the three electrodes. The shaded area indicates the redox probe solution.

1.1.2 Nyquist Plot

The data obtained following an EIS experiment can be plotted as a Nyquist plot. The expression for impedance (Z) is composed of real (Z_{re}) and imaginary (Z_{im}) parts. The imaginary part is due to capacitative effects of the alternating current frequency and the real part is simply due to resistance. If Z_{re} is plotted on the X axis and the negative of Z_{im} on the Y axis, a Nyquist plot is obtained. The Nyquist plot for a bare electrode (see figure 2) shows a semicircular region at higher frequencies (closer to the origin) on the Z_{re} axis followed by a straight line. In an electrochemical cell composed of a gold surface and a solution with redox probe, the semicircular region of the plot indicates kinetic control over the impedance which is dictated by the properties of the gold surface (typically this will mean the presence or absence of adsorbed molecules), while the straight line corresponds to direct electron transfer through the solution containing the redox probe. Thus, the straight linear portion of the Nyquist plot, obtained at larger values of Z_{re}, represents the diffusion-controlled electron transfer process known as Warburg impedance (Long *et al,* 2003). The resistance of the solution (R_S) is due to the properties of the solution through which the potential is applied and will depend on, among other factors, the ionic strength of the solution. The magnitude of R_S is equal to the value of Z_{re} between the origin and the lowest Z_{re} value of the semicircular portion of the curve. All impedance data shown in the results section are depicted in this manner and the charge transfer resistance (R_{CT}) values referred to in descriptions of data are the Z_{re} values at which Z_{im} reaches a minimum.

1.1.3 Modified Randles Circuit

One advantage of EIS is that a purely electronic model can be used to represent an electrochemical cell. The interface of an electrode undergoing an electrochemical reaction is analogous to an electric circuit consisting of a specific combination of resistors and capacitors. Electrochemical investigations of DNA monolayers on gold surfaces measured with intercalated or soluble redox probes can be modeled after the Randles circuit. In the modified Randles circuit, shown in figure 3, R_S represents the resistance of the solution between the working electrode and the reference electrode. The R_{CT} results from the transfer of the electrons from the redox probe to the DNA monolayer and from the DNA helices to the gold surface of the working electrode. Because of the nature of the relationship between R_{CT}

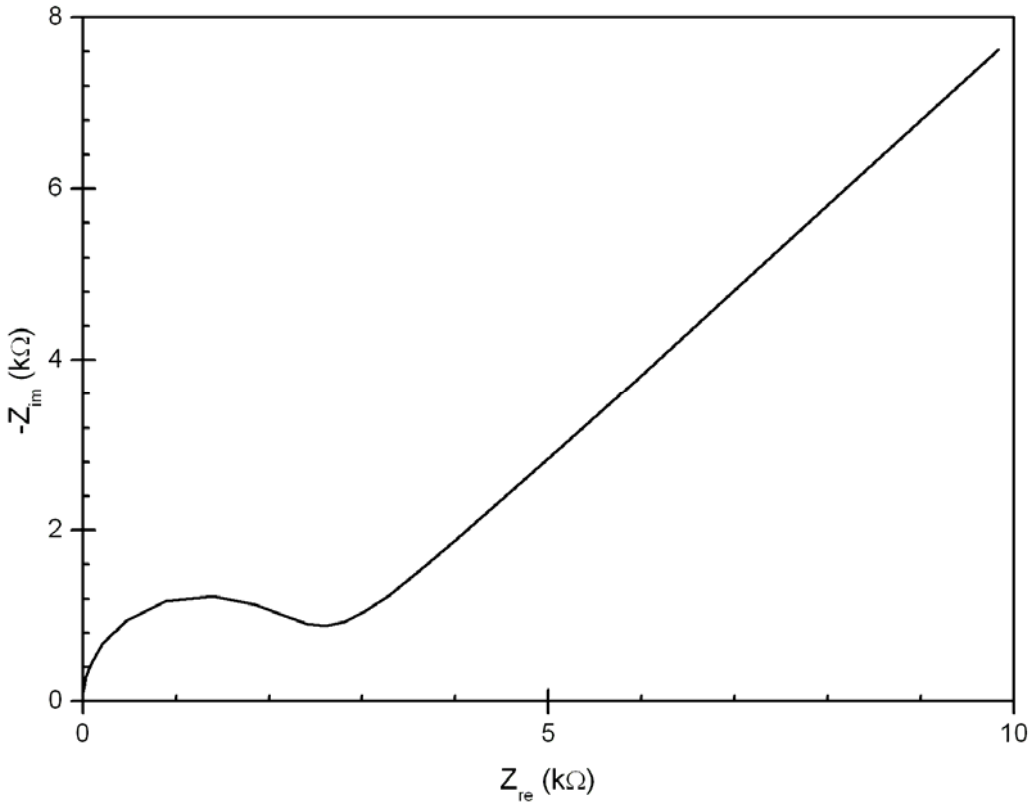

Figure 2: Theoretical Nyquist plot of a bare gold electrode.

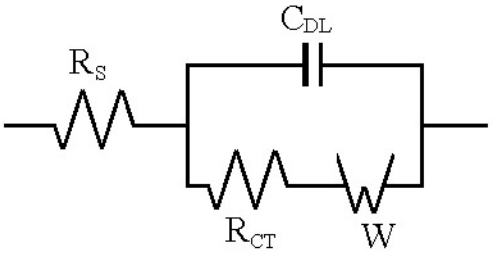

Figure 3: A schematic representation of the modified Randles circuit. The indicated aspects of the circuit are double-layer capacitance (C_{DL}), Warburg impedance (W), charge-transfer resistance (R_{CT}), and solution resistance (R_S).

and the electron transfer between the redox probe and the monolayer, changes in R_{CT} can be used to measure changes in the properties of the monolayer. The C_{DL} is the double layer capacitance of the interface between these two layers. The double layer capacitance is in parallel with the impedance due to the charge transfer reaction. The Warburg impedance (W) depends on the rate of diffusion of the redox probe. A Randles circuit can be used to determine whether W is a significant contributor to the observed impedance, which can help to describe reaction mechanisms in some EIS studies since large dependence on W indicates that the reaction is diffusion limited. The values of W and C_{DL} contribute significantly to the impedance at low frequencies and as the frequency increases, the finite contribution from C_{DL} becomes less significant (Bard and Faulkner, 2001). An "un-modified" Randles circuit differs from the modified Randles circuit shown in figure 3 by the absence in the former of the Warburg impedance component of the system.

1.1.4 Cyclic Voltammetry

Cyclic voltammetry is another electrochemical technique wherein the potential is varied in very small increments in both positive and negative directions. If the potential is greatly positive of the formal potential of the electrode ($E^{0`}$) and adjusted negatively, reduction begins once the potential reaches the vicinity of $E^{0`}$ and the current starts to flow. As the potential moves towards $E^{0`}$, the surface concentration of the electrode material begins to deplete as it is oxidized and the un-oxidized electrode material below the surface begins to move towards the surface by mass transfer. As this mass transfer rate increases, the current also increases. Once the potential moves past $E^{0`}$ to more negative values, the mass transfer and the current reach a maximum and then decline due to depletion of oxidized species at the surface. Without oxidized species of electrode material at the surface, the impetus for mass transfer of un-oxidized electrode material is removed. If the potential is then adjusted to move towards more positive values, the reduced species will be oxidized as the current again approaches $E^{0`}$ and the reverse process occurs with a maximum current being observed at potentials slightly positive of $E^{0`}$ and then dropping off due to depletion of the reduced species at the surface (Bard and Faulkner, 2001)**.** A typical example of a cyclic voltagram is shown below in figure 4.

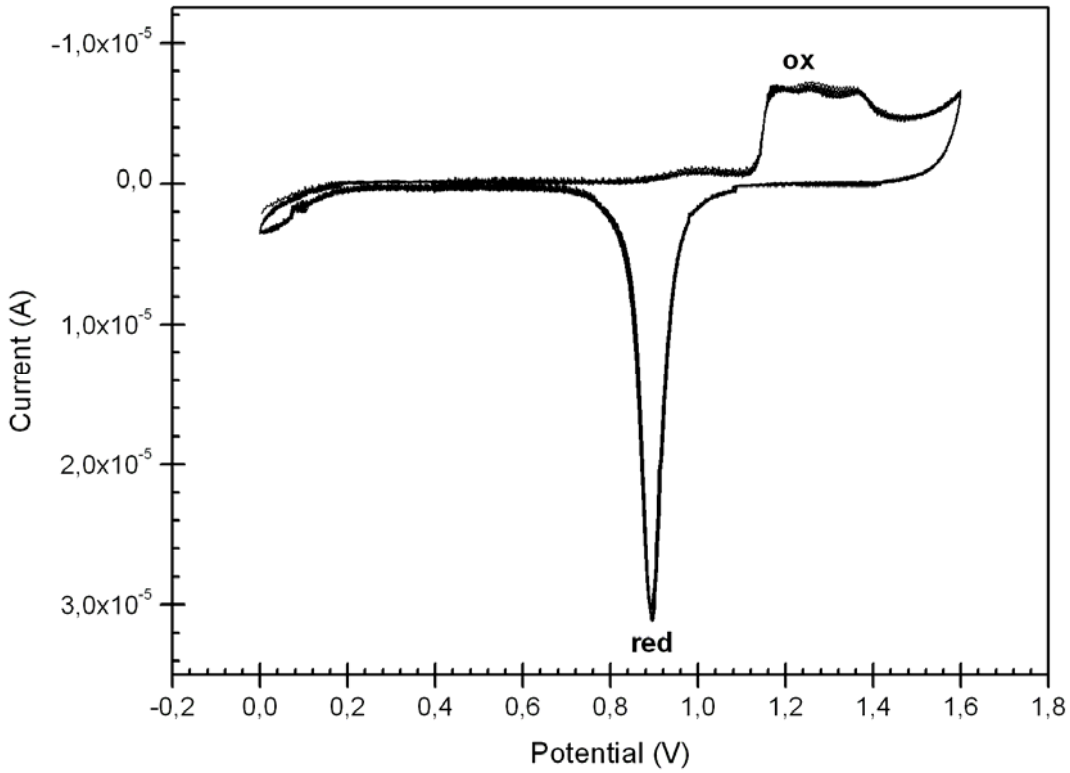

Figure 4: A cyclic voltagram for a bare gold electrode. The oxidation and reduction peaks are indicated by **ox** and **red**, respectively.

1.2 DNA Structure

The EIS spectrum obtained from a monolayer of dsDNA bonded to a gold surface will to some extent be determined by the structure of the DNA molecules making up the monolayer. An individual strand of DNA is composed of multiple nucleotides. Each nucleotide contains a nitrogenous base, a pentose and a phosphate. A base and a pentose form a nucleoside. The bases can be purines: adenine (A) and guanine (G), or pyrimidines: cytosine (C) and thymine (T). The pentose in DNA is 2'-deoxy-D-ribose, while the pentose in RNA is D-ribose. The structures of each base and of 2'-deoxy-D-ribose are shown in figure 5 (Watson and Crick, 1953).

The structure of double-stranded DNA (dsDNA) was elucidated by analyzing DNA structure with X-ray fibre diffraction. In its most common conformation, B-DNA, a DNA molecule is comprised of two strands that form a right-handed double helix by coiling around the same axis. The strands are antiparallel, which signifies that their 5',3'- phosphodiester bonds go in opposite directions. The strands are also complementary, meaning their base sequences are not identical, but complement each other (ie, A bonds with T and G bonds with C). On the outside of the double helix there are the negatively charged phosphate groups and the hydrophilic regions of the pentoses. The hydrophobic regions of the bases are inside the double helix. The complementary nature of the interactions between the two strands of a DNA helix is determined by the bases present on each strand, and specificity in the interactions between the two strands is determined by hydrogen bonding; A interacts with T and G interacts with C as shown in figure 6 (Watson and Crick, 1953). The conformation of the two strands creates a major and a minor groove in each base pair as shown in figure 6. The major and minor grooves can be of different relative sizes depending on the conformation of the DNA and can be important structural determinants in interactions between DNA and proteins (Sinden, 1994). DNA strands can be separated by increasing the temperature or by lowering the ionic strength of a solution of dsDNA (Marmur and Doty, 1962). Conversely, by exposing complementary DNA strands to each other in solution, dsDNA can be formed since the strands recognize each other and hybridize.

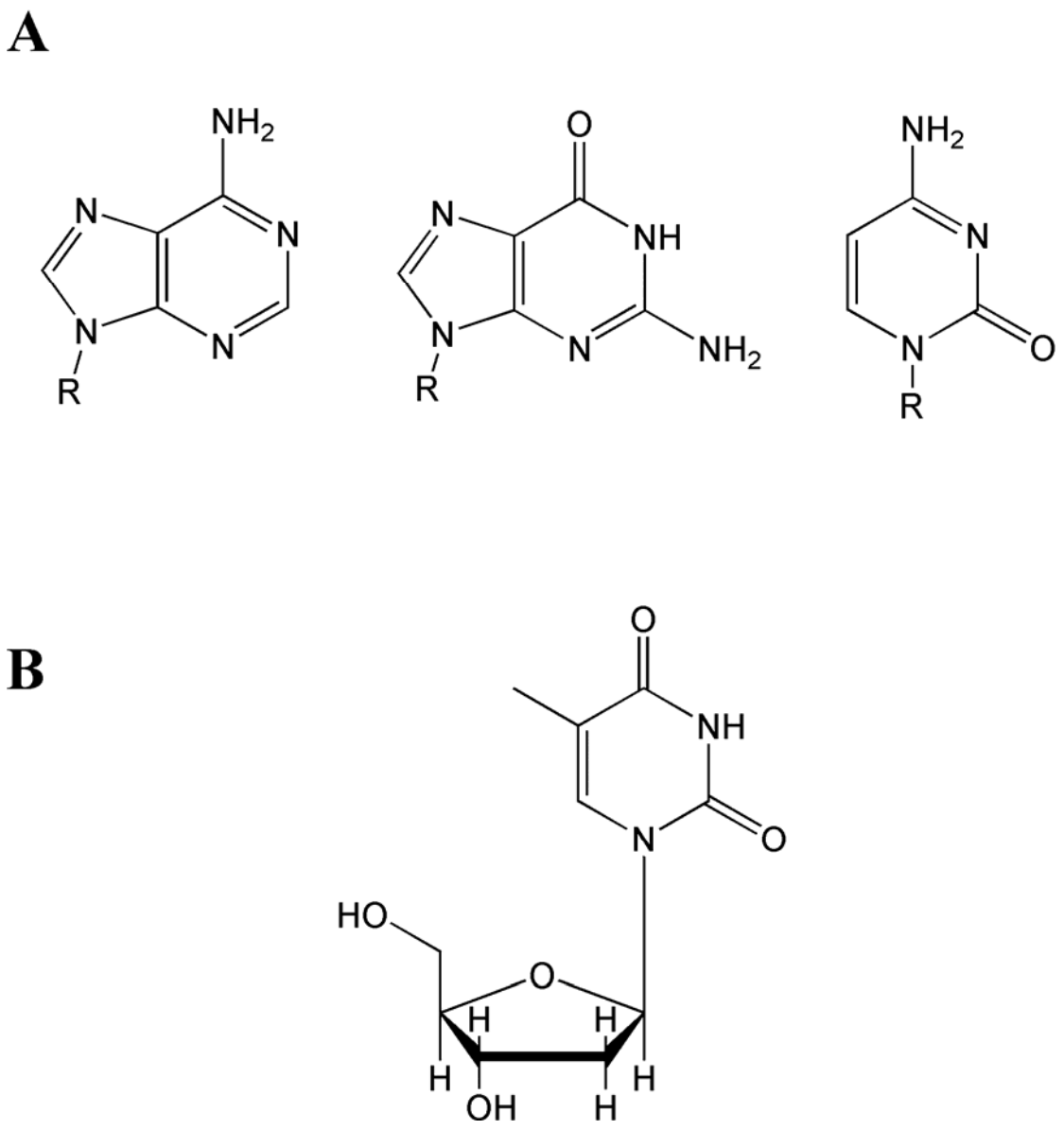

Figure 5: The structures of adenine, guanine, and cytosine, respectively, where R is a proton (**A**) and of thymidine, which contains the 2'-deoxy-D-ribose sugar moiety of a nucleoside (**B**). Any of the bases in (**A**) can be attached to 2'-deoxy-D-ribose at the position indicated as R in (**A**) to form adenosine, guanosine, and cytidine, respectively.

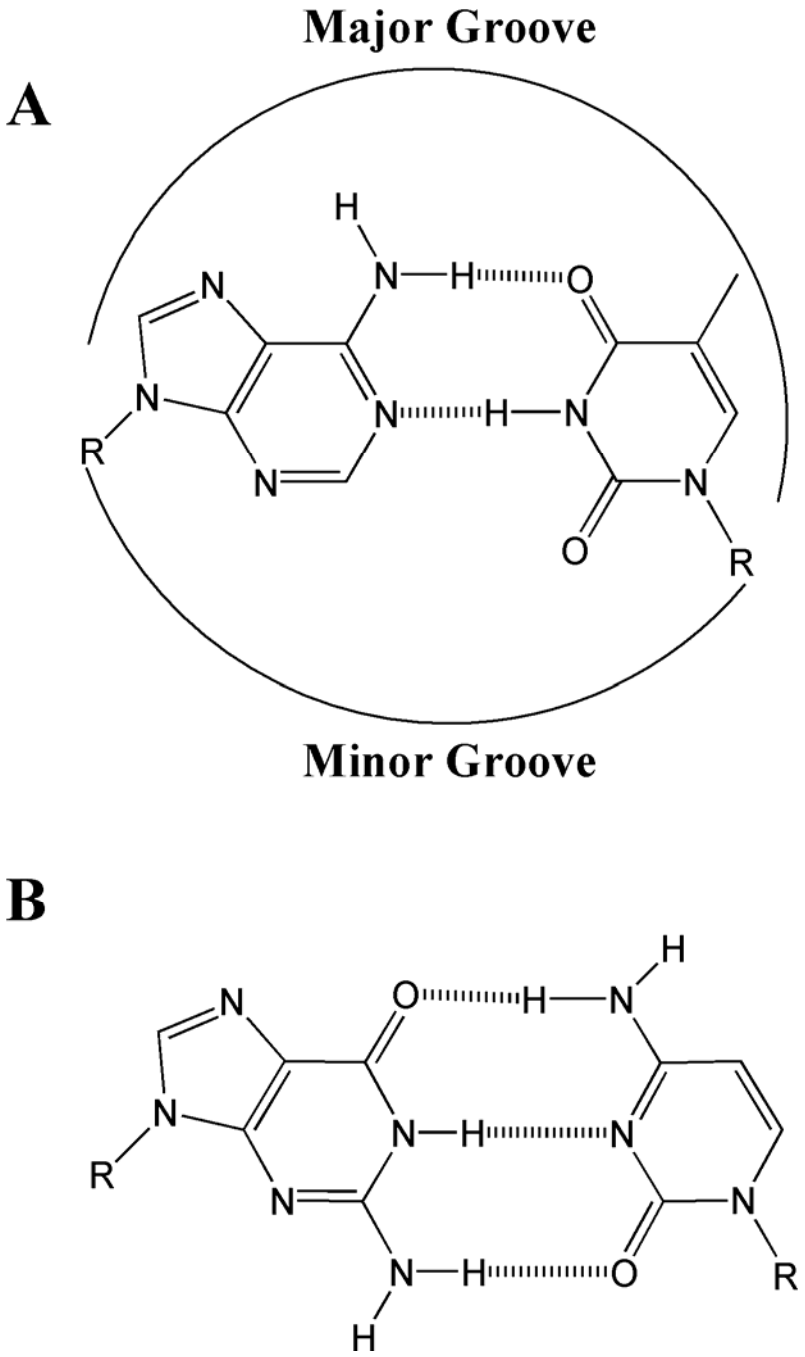

Figure 6: Base pairing between A and T (**A**) and between G and C (**B**). The locations of the major and minor grooves are indicated in (**A**) and are also present in the analogous positions in (**B**).

1.2.1 DNA-binding Molecules

The structure of DNA presents a variety of sites where ligands may interact to bind to the DNA. The major categories of non-covalent binding to DNA are ionic interactions with the phosphate backbone, hydrophobic intercalative binding with the bases, and mixed interactions with the major or minor grooves. Spermine, polylysine, actinomycin D, and proteins each bind to DNA through one or more of these binding mechanisms.

1.2.1.1 Spermine

There are many small molecules that can interact with DNA in a physiologically relevant fashion. A major family of these compounds is the polyamines. Polyamines such as spermine are polycationic aliphatic compounds found in all cells that play a role in the regulation of cellular proliferation (Tabor and Tabor, 1984). Light scattering studies have shown that spermine causes DNA condensation, likely due to neutralization of the negative charges on the phosphate backbone, which in turn lowers the ionic repulsion between individual strands and allows the DNA to adopt a more compact shape (Wilson and Bloomfield, 1979). Although spermine causes condensation of DNA, Raman spectroscopy studies demonstrated that other than condensation, the impact of spermine binding on the secondary structure of B-DNA was negligible (Deng *et al*., 2000). Spermine binding can facilitate a B-DNA to Z-DNA transition, but this is dependent on the DNA sequence being appropriate for formation of Z-DNA (Basu *et al*., 1987). Spermine binding can also facilitate a B-DNA to A-DNA transition, but this is similarly dependent on low humidity (Minyat *et al*., 1978). Spermine is a tetravalent polyamine found *in vivo* in the nuclei of cells, while spermidine is a trivalent polyamine. Polyamines with more positive charges per molecule facilitate DNA condensation at lower concentrations that those with fewer positive charges per molecule (Wilson and Bloomfield, 1979). The structure of spermine in its fully protonated state at physiological pH is shown in figure 7.

The mechanism of spermine binding to DNA has been the subject of a number of studies. Early theoretical work suggested that spermine binds in the major groove through ionic interactions between the proton donors on spermine and the proton acceptors either on N7 of purines or on the phosphate backbones of the DNA (Feurstein *et al*., 1986). Subsequent simulations suggested that spermine binds to the major groove of $(dGdC)_5$•$(dGdC)_5$, but

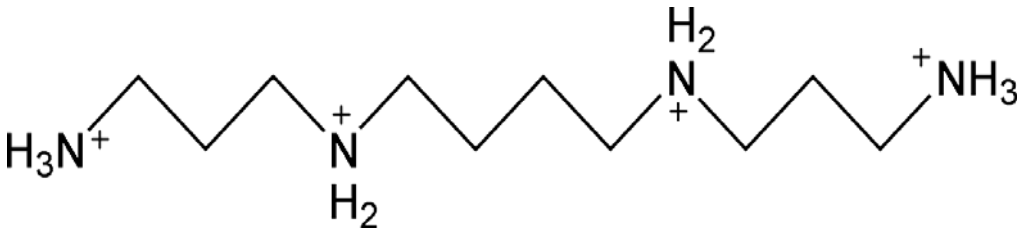

Figure 7: The structure of spermine. Note that at neutral pH it has 4 positive charges.

interacted non-specifically with the phosphate backbone of $d(G)_{10}$•$d(C)_{10}$ (Feurstein *et al*., 1989). Later DNA footprinting studies suggested that spermine binds to the minor groove of DNA, weakly favours AT rich DNA, and that the spermine molecules were highly mobile within the minor groove. These footprinting studies also showed spermine to bind in the major groove when binding to A-DNA, but not when binding to B-DNA (Schmid and Behr, 1991). Thus, there is some controversy as to whether spermine binds in the major or minor groove of B-DNA or possibly both.

Raman spectroscopy suggests that the backbone phosphates are the primary site of interaction between DNA and spermine, and that major groove sites play only a secondary role. The secondary role of the major groove proton acceptors explained the weak sequence specificity of spermine (Deng *et al*., 2000). Another Raman spectroscopy study of interactions between spermine and DNA confirmed the presence of contacts between the phosphate backbone and spermine, as well as contacts between purine N7 positions and possibly the 4-keto group of thymine. These data supported earlier findings that spermine binds preferentially to AT rich regions as compared to GC rich regions of DNA (Ruiz-Chica *et al*., 2001). Later light scattering studies also illustrated that the interaction between spermine and DNA was primarily ionic and therefore likely mediated largely through non-specific interactions between spermine and the phosphate backbone (Vijayanathan *et al*., 2001).

Despite the controversy over the location of spermine when bound to random sequence DNA and the debate over the role of the proton acceptors located in the major groove in determining the binding site of spermine, there are several points of agreement in the literature. First, spermine undoubtedly causes DNA to condense. Second, a strong point of contact between spermine and DNA is the phosphate backbone of DNA. Third, unless the DNA has a base sequence suitable for forming Z-DNA or is present in a dehydrated solution, spermine binding has little impact on DNA conformation other than condensation.

1.2.1.2 Polylysine

Polylysine is a positively charged peptide at neutral pH and is formed through amide linkages typical of any other polypeptide. Polylysine can be of any length and the structure of an oligolysine molecule four residues long is shown below in figure 8. Polylysine binds polynucleotides through interactions between positively-charged amines on the lysine R groups and negatively-charged phosphates on the backbone of a polynucleotide (Sober *et al*., 1966; Latt and Sober, 1967). Studies on the ionic strength dependency of polylysine

interactions with single-stranded DNA (ssDNA) have shown the interaction to be primarily due to the increase in entropy that occurs upon binding. The increase in entropy is due to release of counterions from the DNA during binding (Mascotti and Lohman, 1990). Electron microscopy studies have shown the binding process to be cooperative in the presence of excess DNA and at high NaCl concentrations, with some DNA molecules entirely condensed and others unbound. Conversely, at low NaCl concentrations the binding is non-cooperative with polylysine randomly binding different DNA molecules (Liu *et al*., 2001).

Upon binding with polylysine, dsDNA collapses into either a donut or short stem shape. The change in shape prevents degradation of the DNA by endonucleases (Laemmli, 1975; Wagner *et al*., 1991). A fluorescence-based study of DNA condensation showed polylysine to condense DNA to a lesser extent than spermine, with individual DNA molecules being more isolated from other DNA molecules than was observed in condensation by spermine (Trubetskoy *et al*., 1999). Effective condensation of DNA and nuclease resistance imparted by this condensation was observed under cooperative binding conditions, but not under non-cooperative binding conditions (Liu *et al*., 2001).

1.2.1.3 Actinomycin D

Actinomycin D was one of the first cytotoxic drugs to be used as an anti-cancer drug. The cytotoxicity of actinomycin D was attributed to its apparent ability to bind to DNA by intercalation, thus interfering with synthesis and function of DNA (Wadkins *et al*., 1996). Actinomycin D is composed of two pentapeptide lactone rings composed of L-Threonine, L-Methyl-Valine, N-methyl-glycine, L-proline, and D-valine attached to a phenoxazone ring through amide linkages. Both the phenoxazone ring and the lactone rings have been implicated in binding of the drug to DNA. The structure of actinomycin D is shown below in figure 9.

NMR and molecular dynamics studies have demonstrated that the phenoxazone ring of actinomycin D binds to dsDNA through stacking interactions at and between intercalation sites and through intermolecular hydrogen bonds. The three rings in the phenoxazone portion of actinomycin D interact with both guanine residues in the (dGdC)•(dGdC) sites, which contributes to the specificity of actinomycin D for this sequence. The phenoxazone rings intercalate between bases when actinomycin D binds to DNA. In addition, the phenoxazone ring NH_2 group participates in hydrogen bonding with the O4' and O3' of the residues between which it is intercalated. This last mode of binding is not sequence specific and may

.

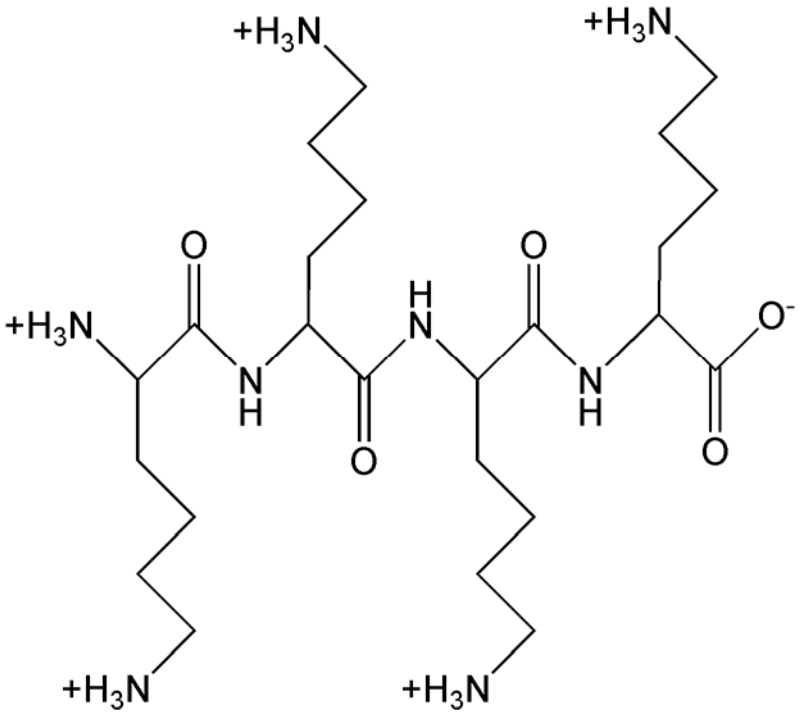

Figure 8: A polylysine molecule containing four lysine residues. The R groups are positively charged at physiological pH.

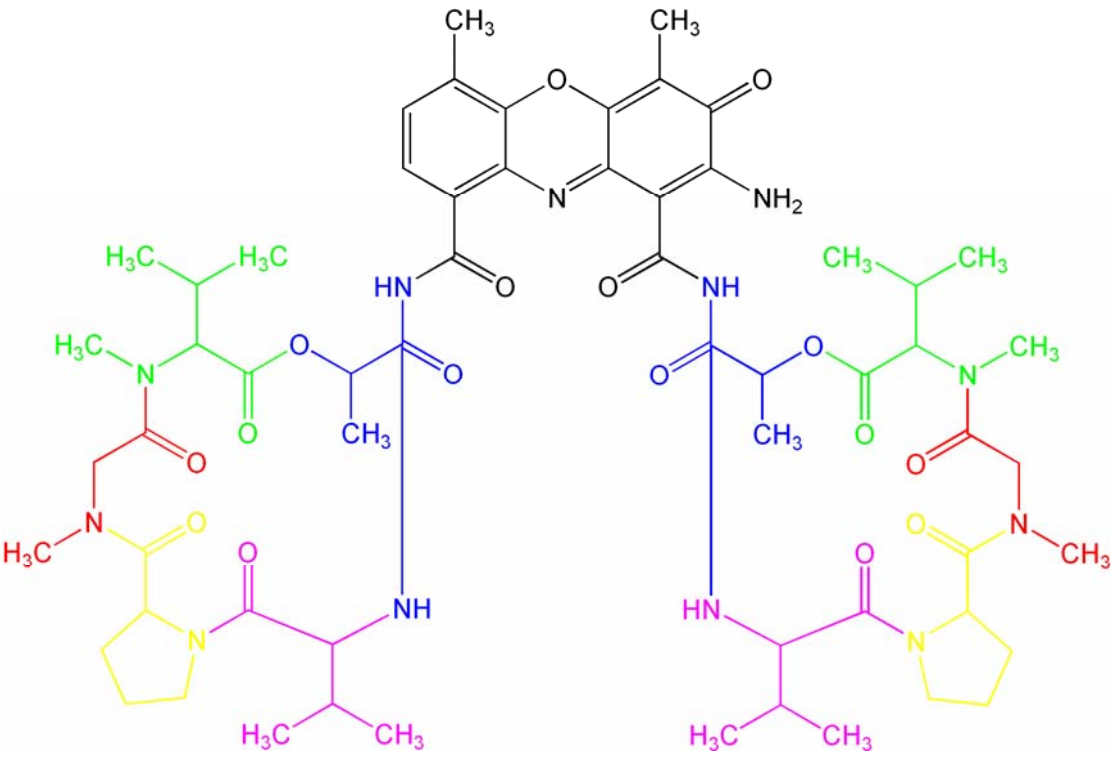

Figure 9: The structure of actinomycin D. The peptide residues in the lactone ring are colour-coded: L-threonine (blue), L-methyl-Valine (green), N-methyl-glycine (red), L-proline (yellow), and D-valine (purple). The phenoxazone ring is drawn in black.

be involved in initial binding of actinomycin D to DNA before it binds to the DNA at its preferred sequence (Chen *et al*., 1996).

The same NMR and molecular dynamics studies that illuminated the role of the phenoxazone ring in intercalation and hydrogen bonding have demonstrated that both lactone rings participate in hydrogen bonding with the bases in the minor groove. The lactone rings project in opposite directions from the intercalated phenoxazone ring into the minor groove. Intermolecular hydrogen bonds between the lactone rings and the minor groove of the DNA contribute to the sequence specificity of actinomycin D for (dGdC)•(dGdC) sites. The strongest hydrogen bonds observed were between the carbonyl portions of the backbone of L-Thr and the exocyclic NH_2 protons on guanine. The weaker hydrogen bonds observed were between the amide portion of the backbone of L-Thr on the lactone rings of actinomycin D and N3 on the guanine residues in the minor groove. Binding of actinomycin D widens the minor groove to up to 19.4 Å as compared to roughly 6 Å in native B-DNA, with the width of the minor groove being defined as the shortest interstrand phosphorous-phosphorous minus 5.8 Å (Chen *et al*., 1996).

Binding of actinomycin D to native B-DNA in solution has also been observed with cyclic voltammetry and this study confirmed that the phenoxazone ring was intercalating between base pairs and that the lactone rings extend along the minor groove of the DNA covering eight base pairs (Wang *et al*., 2003a). Another study by the same group showed the binding constant of actinomycin D for calf thymus DNA to be 9.1×10^9 mL/mol (Wang *et al*., 2003b).

NMR studies suggest that 7-amino actinomycin D, a fluorescent analogue of actinomycin D, also binds to ssDNA by "hemi" intercalation between adjacent purine bases; the "hemi" designation is simply to distinguish this mode of binding from intercalation into dsDNA. Fluorescence spectroscopy studies have shown actinomycin D to be sequence-specific when binding to ssDNA, with the sequence TAGT binding the drug most strongly. The sequences AGT, AGA, and TGT also bound actinomycin D, but the sequence TGA did not show any significant binding. The strength of the interaction between DNA and actinomycin D was also strongly affected by the length of the sequences flanking the binding sequence (Wadkins *et al*.,1996). In summary, actinomycin D binds to both dsDNA and ssDNA, with a specificity for (dGdC)•(dGdC) sites in dsDNA and although showing less specificity in ssDNA, a preference for the sequence TAGT, but a failure to bind TGA.

1.2.1.4 Protein-DNA Interactions

Proteins such as transcription factors, steroid receptors, and protein components of ribosomes bind to DNA in a sequence-dependent way. Such sequence-dependent interactions are primarily mediated through hydrogen bonds, hydrophobic interactions, and ionic interactions with the phosphate backbone. Sequence-dependency is achieved through precise positioning of peptide and nucleoside residues involved in hydrogen bonding when the protein and the DNA are in close proximity. For example, a common interaction found in DNA-binding proteins is between an arginine residue on the protein and a guanine residue in the major groove; such a contact is illustrated in figure 10. A particular combination of several intermolecular interactions between residues of a given protein and a given DNA sequence will ensure that the protein only binds tightly to the DNA sequence to which it is targeted. The more points of contact that exist between a DNA-binding protein and a DNA sequence, the more specific the interaction will be (Luscombe *et al*. 2001).

In addition to specific interactions between DNA and antibodies or DNA-binding proteins, some proteins interact with DNA through non-specific ionic interactions. Bovine serum albumin (BSA) is a readily obtainable, inexpensive protein frequently used in biochemistry. Albumin is the most abundant protein in the circulatory system, contributing to colloid osmotic blood pressure (Carter and Ho, 1994). Albumin is also important for the maintenance of blood pH (Figge *et al.*, 1991). The binding of BSA to a DNA monolayer was assayed by cyclic voltammetry and it resulted in no modification of the signal since BSA does not interact with DNA due to the repulsion between their negative charges (Boon *et al.*, 2002). Native BSA has an overall charge of -18, but esterification of the carboxyl groups on amino acid side chains by exposure of the protein to methanol under acidic conditions produces methylated BSA (me-BSA) (Fraenkel-Conrat and Olcott, 1945), which is positively charged with a pI of 8.5 (van den Berg *et al.*, 1984). Thus, me-BSA can bind DNA through ionic interactions with the phosphate backbone. In the past, this interaction has been exploited in the production of columns used to purify DNA (Masamune, 1964).

1.3 Immobilization of DNA to Gold Surfaces

Adsorption of disulphides to gold is recognized to be superior to that on silver because clean gold surfaces are easy to prepare by vacuum evaporation and the surfaces are generally resistant to contamination under laboratory conditions. Additionally, silver surfaces tend to

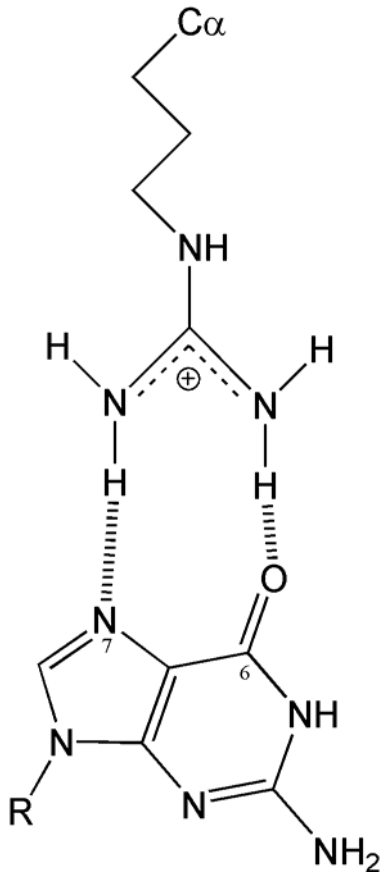

Figure 10: An example of specific binding in the major groove that can occur at physiological pH. The protonated R group on an arginine residue acts as an electron acceptor in hydrogen bonds, while the 6-keto and 7-imino positions on guanine act as electron donors.

cleave both S-S and C-S bonds, while gold surfaces leave C-S bonds intact. This latter property of gold surfaces enhances the reproducibility of binding disulphide-labelled biological molecules such as DNA to gold surfaces as compared to silver surfaces (Nuzzo and Allara, 1983). When biomolecules are attached to gold surfaces, identical S-Au linkages are formed regardless of the sulphur atom being part of a thiol or a disulphide, although thiols bind to the gold surface more readily than disulphides (Bain *et al*., 1989). Studies have also shown that when a disulphide of the form R_1SSR_2 is exposed to a gold surface, both Au-SR_1 and Au-SR_2 are formed and are formed in equal proportion regardless of the specific R groups, although the stability of the bonds is affected by the specific R groups (Biebuyck and Whitesides, 1993).

Driven by a demand for reproducible gold chips with immobilized DNA for use as biosensors based on fluorescence, radiolabelling, surface plasmon resonance, or quartz crystal resonance, a large volume of work has been done on characterizing the binding of thiol-labelled DNA to gold surfaces through S-Au bonds (Herne and Tarlov, 1997). Cyclic voltammetry studies have shown that ssDNA molecules shorter than 24 bases organize in end-tethered arrangement with strong long-term stability, while longer ssDNA had less coverage and were less stable. The behaviour of the longer DNA molecules was believed to be due to a less ordered arrangement reflecting increasingly polymeric behaviour (Steel *et al*., 2000).

1.3.1 Dilution of DNA Monolayers by Alkanethiols

In addition to the desired Au-S bonds formed when thiol-labelled DNA (single-stranded or double-stranded) is exposed to a gold surface, the DNA will also bind in other, non-specific ways to the surface. These undesired bonds between the gold and the DNA can be reduced by exposure of the DNA monolayer to an alkyl thiol. Alkanethiols bind to the gold surface, diluting the DNA monolayer and allowing the antibodies or other proteins better access to the DNA (Li *et al*., 2003). As with formation of monolayers of thiol or disulphide-labelled biomolecules, the formation of self-assembled monolayers (SAM) of alkanethiols involves cleavage of the S-H bond and formation of a Au-S bond as follows for the example of butanethiol (Truong and Rowntree, 1995):

$$CH_3(CH_2)_3SH + Au \longrightarrow CH_3(CH_2)_3SAu + \tfrac{1}{2} H_2 \qquad (1.1)$$

Such treatment has the effect of diluting the DNA monolayer and removing the non-specifically bound DNA molecules and improves the reproducibility and stability of ssDNA

monolayers for hybridization and dehybridization experiments (Herne and Tarlov, 1997). Hybridization studies using cyclic voltammetry have shown that when a ssDNA monolayer is diluted by an alkylthiol spacer, the hybridization efficiency increases with increasing ssDNA surface concentration. Surface concentrations of up to 10^{13} molecules per cm^2 were observed (Steel *et al*., 1998).

A variety of DNA-protein interactions have been probed by electrochemical methods. In one study, several test proteins bound to a DNA monolayer causing a modification in the charge transport through DNA (Boon *et al.*, 2002). In this study, the redox-active intercalator daunomycin was covalently bound to the top of the DNA monolayer to provide a redox probe for cyclic voltammetry. Another study employed cyclic voltammetry to measure the interaction between DNA and an anti-DNA IgM; a decrease in the current was observed upon binding of the IgM (Katayama *et al*., 1998). In the two above-mentioned studies, mercaptohexanol and 2-mercaptoethanol were used, respectively, to bind to the exposed gold surfaces and thus prevent proteins or redox probes from interacting directly with the gold surface. Work in our lab has shown that upon binding the protein MutS, the impedance of a DNA monolayer increased. Binding of MutS to DNA was facilitated in this study by dilution of the dsDNA monolayer by butanethiol.

1.4 Immunology

1.4.1 Antibody Structure

An antibody molecule contains four distinct polypeptides of two different types: two identical light chains each approximately 24 kDa in size and two identical heavy chains each approximately 55 to 70 kDa in size. The size of the heavy chain depends on the class of antibody and immunoglobulin G (IgG) molecules will be approximately 150 kDa. The heavy chains are joined to each other through disulfide bonds between oxidized cysteine residues, while each light chain is joined to one heavy chain through the same type of bond (Haynes and Fauci, 2005). The general structure of an IgG is shown in figure 11.

Both light and heavy chains are composed of constant and variable regions. The constant regions will be similar for all antibodies of a given allotype, while the variable regions are distinct on antibodies of varying idiotypes. The constant regions of antibodies are recognized by and interact with effectors in order to produce the correct immune response, while the variable regions of antibodies interact with the antigen recognized by a given

antibody (Haynes and Fauci, 2005). The variable regions of the heavy and light chains together will bind to the antigen recognized by an antibody; this portion of the antibody is the antigen binding fragment (Fab) and can be separated from the remainder of the antibody by digestion with the enzyme papain. If two distinct antibodies recognize the same antigen, it is likely that they bind to different portions of the antigen. This difference will be due to differences in the variable regions of the heavy and light chains of the two antibodies**.** The particular way in which an antibody recognizes and binds to an antigen defines the antibody's idiotype. Antibodies are produced by B lymphocytes, often stimulated by T lymphocytes. Each B lymphocyte is capable of expressing one antibody of a specific idiotype and allotype. All B lymphocytes have a receptor identical to the idiotype of the antibody that the cell is capable of expressing (Haynes and Fauci, 2005).

1.4.2 Autoimmune Diseases

Autoimmune diseases are a family of diseases wherein lymphocytes are activated in the absence of pathogens. Immune reactions based on antibody- or cell-mediated defence mechanisms occur against the individual's body either systemically or against particular cells or organs. Autoimmunity can arise when lymphocytes encounter antigens that are rarely encountered by lymphocytes (Lipsky and Diamond, 2005). Some targets for autoimmune reactions are cardiolipin, carbonic anhydrase II, collagen, dsDNA, golgin, histone H2A-H2B-DNA, Ku-DNA-protein-kinase, and RNA polymerase I-III among others in systemic lupus erythematosus (SLE) and carbonic anhydrase II, golgin, IgA, and La phosphoprotein among others in Sjögren's Syndrome (Haynes and Fauci, 2005). SLE often involves arthritis that varies from mild to disabling and 10% of cases show joint deformities. SLE symptoms can affect the skin, kidneys, nervous system, circulatory system, lungs, heart, blood, gastrointestinal system, and eyes of patients. Sjögren's Syndrome can also affect the eyes of a patient, sometimes causing blindness. SLE can in some cases be life-threatening and in such cases is treated with both high dose glucocorticoids and cytotoxic drugs (Hahn, 2005).

Individual autoimmune diseases are themselves very heterogeneous and present a significant diagnostic challenge because many of their features overlap. Many of these diseases are characterized by the presence of circulating antibodies against a variety of autoantigens that could potentially be used as a diagnostic tool (Eilat, 1982; Shoenfeld *et al.*, 1983). For example, in SLE antibodies to DNA are present with anti-duplex DNA antibodies

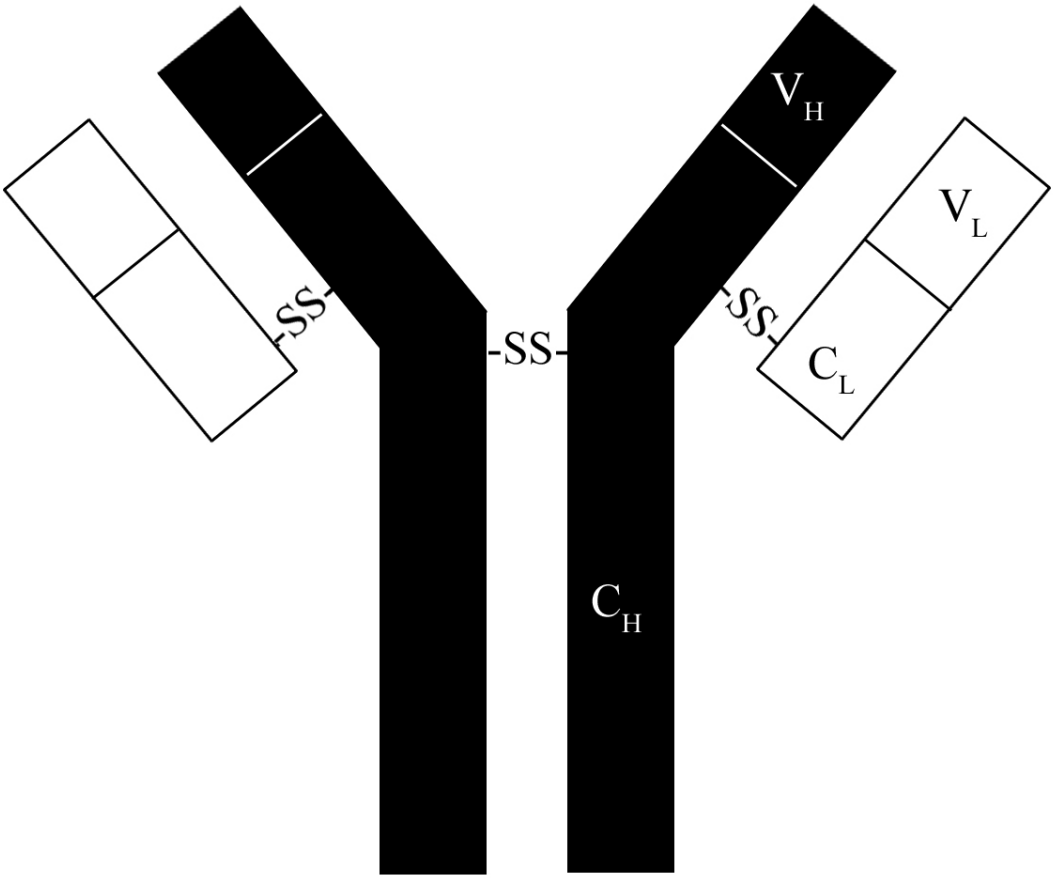

Figure 11: The general structure of an IgG. The heavy chains are black while the light chains are white. Note the presence of S-S covalent bonds between light and heavy chains and between heavy chains. The variable and constant portions of the heavy chains are indicated by V_H and C_H, respectively while variable and constant portions of the light chains are indicated by V_L and C_L, respectively. Adapted from Haynes and Fauci, 2005.

correlating with a poor prognosis. Sjögren's syndrome may also be characterized by the presence of antibodies specific for RNA (Haynes and Fauci, 2005). As with any progressive disease, early diagnosis will often improve the prognosis. Thus, a rapid and sensitive assay for the presence of antibodies specific for DNA would be a valuable diagnostic tool for physicians treating SLE and other autoimmune disease patients. This assay would have to be sensitive enough to rule out possible non-specific interactions with other serum proteins and if it were rapid enough to be carried out in less than one hour, the possibility of early diagnosis in one visit would be greatly increased. Thus, electrochemical techniques have great potential for creating a useful and practical diagnostic tool in the treatment of autoimmune diseases.

1.4.3 DNA-binding Antibodies

DNA is typically not immunogenic unless it has an unusual conformation (Lafer *et al.*, 1981; Moller *et al*, 1982; Lee *et al*, 1987). Antibodies specific for dsDNA have been implicated in the pathogenesis of SLE (Koffler, 1974; Tsao *et al.*, 1990) The origins of these antibodies are unclear, but it is unlikely that they arise in response to dsDNA owing to its low immunogenicity (Stollar, 1994). New Zealand Black (NZB) and New Zealand White (NZE) mice, which have been used as models of SLE, have antibodies specific for dsDNA in their serum (Tsao *et al.*, 1990; Braun and Lee, 1986). Different antibodies specific for dsDNA (Braun and Lee, 1986; Tanha and Lee, 1997), ssDNA (Lee *et al*., 1982), or both (Swanson *et al*., 1996) have been isolated from various strains of lupus-prone mice. These antibodies have varying degrees of sequence-specificity (Braun and Lee, 1986).

1.4.3.1 Jel 72

Jel 72 is an immunoglobulin G that was originally produced by immunizing C57 black mice with poly(dG)•poly(dC). Jel 72 is specific for poly(dG)•poly(dC) and shows reduced binding to similar DNA sequences comprised of either standard bases or structural analogues of guanine or cytosine. Similarly, Jel 72 shows minimal binding to poly(dG)•poly(dC) where guanine and cytosine are replaced with structurally analogous bases. The binding strength of Jel 72 to poly(dG) rich DNA was 0.7 of its binding to poly(dG)•poly(dC) (Lee *et al*., 1984).

Jel 72 does not bind to single-stranded or multi-stranded DNA structures. It is unlikely that poly(dG)•poly(dC) was adopting an unusual DNA conformation under the experimental conditions wherein its binding was characterized (Lee *et* al., 1984). The conformation

adopted in solution by poly(dG)•poly(dC) is one with a deep and narrow major groove and a wide and shallow minor groove. The conformation of poly(dG)•poly(dC) is very similar to the classical A-DNA conformation (McCall *et al*., 1985). It is likely that Jel 72 recognizes this conformation.

The Fab fragments of Jel 72 have been crystallized (Boodhoo *et al*., 1988) and the crystal structure has been solved to 2.7 Å (Mol *et al*., 1994). The initial solution of the Jel 72 Fab structure suggests that amino acid residues in the third hypervariable region of the heavy chain interact with the DNA bases in the major groove of poly(dG)•poly(dC). There were also apparent interactions between the third hypervariable region and the DNA phosphate backbone. Hydrogen bonds between the amino groups of arginine residues as proton donors and the N7 and O6 of guanine residues as proton acceptors account for the high degree of specificity shown by Jel 72 (Mol *et al*., 1994). Computer modelling of the structure showed that the antigen binding portion of Jel 72 has a relatively flat surface which contacts the DNA in its major groove (Barry *et al*., 1994).

1.4.3.2 Jel 274

Jel 274 is a clone of Jel 229, which is an immunoglobulin G originally isolated from NZB autoimmune mice. For simplicity, the antibody will be referred to as Jel 274 regardless of whether it was referred to as Jel 229 or Jel 274 in any given publication. Jel 274 binds dsDNA in the common B-DNA conformation and has a preference for DNA sequences rich in G•C base pairs. Jel 274 binds to *Escherichia coli* DNA, which is 50% GC, 1.2 times as strongly as it does to calf thymus DNA, which is 42% GC. Similarly, Jel 274 binds to *Clostridium perfringens* DNA, which is 30% GC, only 0.70 times as strongly as it does to calf thymus DNA. An exception to this trend is *Micrococcus luteus* DNA, which is 70% GC and yet Jel 274 binds 0.93 times as strongly as it does to calf thymus DNA. Despite the anomalous result with *Micrococcus luteus* DNA, Jel 274 displays a general preference for GC rich sequences, but will bind significantly to any DNA sequence (Braun and Lee, 1986). Jel 274 has a variable heavy domain sequence homology of 84% with Jel 72. Modelling studies have shown that Jel 274 likely binds to DNA in a similar way to Jel 72, with arginine residues in the third hypervariable loop interacting with guanine bases and giving Jel 274 some sequence specificity. The same modelling studies have also shown that the second hypervariable loop of Jel 274 interacts with the minor groove of the DNA (Barry *et al*., 1994). An interaction in the minor groove is consistent with earlier work wherein Jel 274 was observed to bind

significantly to DNA containing putrescinyl thymine residues, which prevent binding in the major groove (Braun and Lee, 1986). That the major groove recognition is not required for binding is consistent with a model for Jel 274 binding that relies primarily on interactions with the phosphate backbone, as suggested by fluorescence quenching studies under variable ionic strength (Tanha and Lee, 1997); this is particularly compelling in light of the low sequence specificity in Jel 274 binding (Braun and Lee, 1986).

1.4.3.3 Hed 10

Hed 10 is an IgG that was originally extracted from autoimmune NZB and NZW mice. Cells secreting Hed 10 have been successfully incorporated into hybridoma cell lines. Hed 10 binds preferentially to ssDNA as compared to dsDNA and has a preference for single-stranded sequences with a high proportion of pyrimidines, as demonstrated through use of the solid phase radioimmunoassay (Lee *et al*., 1981). The specificity of Hed 10 was further investigated in tryptophan fluorescence quenching studies of Fab fragments from Hed 10. Hed 10 was found to recognize four consecutive thymine residues, with two phosphate groups being involved in the binding. Studies on halogenated polydeoxyribonucleotides and on unhalogenated polyribonucleotides implicated the involvement of the 3, 4, and 5 positions of the pyrimidine ring and the deoxyribose sugar in the recognition of ssDNA by Hed 10 (Lee *et al*., 1982). Hed 10 binds very strongly to halogenated poly-pyrimidine sequences, which could be due to the high polarizability of these sequences (Lee *et al*., 1981; Lee *et al*., 1982). The exact sequence specificity of Hed 10 remains elusive but it undoubtedly binds to a thymine-rich sequence. It has also been confirmed that the binding of Fab fragments of Hed 10 to DNA is similar to binding of the entire IgG to DNA (Lee *et al*., 1982).

Crystallization studies on Fab fragments of Hed 10 have been successful, with structures being resolved to 3.0 Å resolution (Cygler *et al*., 1987). Another study revealed that the light chain of Hed 10 contributes little to the recognition and binding of the antibody to DNA (Barry and Lee, 1993). A computer modelling study has shown that antibodies which bind preferentially to ssDNA have deep clefts where the antigen can bind. This study showed that Hed 10 has a long cleft parallel to the V_H-V_L interface. This cleft has tyrosine residues which can stack with thymine bases, as well as arginine and lysine residues which can interact with the phosphate backbone of DNA. However, there was no putative role of any amino acid residues in Hed 10 interacting with the deoxyribose sugar suggested by this study (Barry *et al*., 1994).

1.5 Objectives

The goal of this study was to develop electrochemical tests for autoantibodies that can assess the sera of patients for the presence of these antibodies. Such a test would allow a more rapid diagnosis than with current techniques and would allow the physician to initiate treatment earlier, thus leading to a better prognosis. Specifically, a system wherein a monolayer of double-stranded or ssDNA of a defined sequence is bound to a gold electrode suitable for electrochemical study was sought. EIS would be used to verify the integrity and quality of the DNA monolayer. Following characterization of the DNA monolayer, the patient's serum, likely diluted in buffer, would be exposed to the monolayer and EIS would be performed on the surface once more. The changes in EIS spectra would be correlated with binding of antibodies and the response of different DNA monolayers, distinguishing both between double- and single-stranded DNA and between different sequences of either of those species of DNA, would be useful in further characterizing the pathogenesis of autoimmune diseases that gives rise to anti-DNA antibodies. Although this assay was not completed, groundwork that may lead to such an assay was commenced and the results are encouraging.

As controls, interactions between a monolayer of a dsDNA sequence and me-BSA, spermine, and polylysine were studied. Once this system was established and provided reproducible results, the same protocols were applied to studying the interaction between dsDNA and the well-characterized anti-DNA antibodies Jel 72, and Jel 274. The assay was also used to characterize binding between dsDNA and actinomycin D and binding between double- and single-stranded DNA and Hed 10. Although the data obtained in experiments designed to assess binding between DNA and Jel 72 and 274 were less than satisfactory, the data obtained with Hed 10 agreed well with the literature and demonstrated the usefulness of this assay for characterizing the interaction between immobilized DNA and antibodies. This study has thus provided a beginning to the long-term goal of fabricating a system that can be used to distinguish various autoimmune diseases by assessing the binding of a patient's serum to monolayers of double-stranded or ssDNA of varying sequences.

2.0 Materials and Methods

2.1 Reagents and Equipment

Item	Supplier
Biological Reagents	
Bovine Serum Albumin	Sigma
Calf Thymus DNA (type I: sodium salt)	Sigma
Hed 10 IgG	Dr. J. Lee; (Lee *et al*., 1981)
Jel 72 IgG	Dr. J. Lee; (Lee *et al*., 1984)
Jel 274 IgG	Dr. J. Lee; (Braun and Lee, 1986)
Kilobase Molecular Weight Ladder (#N3232S)	New England Biolabs
Methylated Bovine Serum Albumin	Sigma
Plasmid pT463-I	Dr. J. Lee; (Lee *et al*., 1989)
Chemical Reagents	
Glacial Acetic Acid	BDH
Actinomycin D 98%	Sigma
Agarose	EM Science
Argon gas	Praxair
Butanethiol 99%	Sigma
Bromophenol Blue	BDH
Ethanol 95%	University of Saskatchewan
Ethidium Bromide	Sigma
Glycerol	BDH
$HClO_4$ 60%	Sigma
H_2O_2 30%	EMD
H_2SO_4 98 %	EMD
KNO_3	Sigma
Millipore Water	Prepared with Millipore Q System per manufacturer's directions
$NaClO_4$	Sigma
NaOH	BDH
Poly-L-Lysine	Sigma
Spermine	ICN Biomedicals
Tris[hydroxymethyl]aminomethane	Sigma

Item	Supplier

Supplies and Equipment

Accumet Basic pH electrode	Fisher
Ag/AgCl reference electrode	Bioanalytical Systems
Alumina polishing pads	Bioanalytical Systems
Disposable fluorescence cuvettes	VWR
Double-junction reference electrode chamber	Bioanalytical systems
Eppendorf tubes, 1.5 mL and 0.5 mL	VWR
1.6 mm diameter electrodes	Bioanalytical Systems
Falcon tubes, 15 mL and 50 mL	VWR
0.45 μm filter discs	Nalgene
F-2500 fluorescence spectrophotometer	Hitachi
Gel electrophoresis apparatus GNA 100	Pharmacia Fine Chemicals
Electrophoresis power supply EPS 500/400	Pharmacia Fine Chemicals
Micropipettors	Eppendorf
Microscope	Walter A. Carveth Ltd.
Millipore Q System	Millipore
Platinum wire, annealed 0.5 mm	Alfa Aesar
Polaroid gel camera	Polaroid
Polishing alumina 7 mL	Bioanalytical Systems
Potentiostat model 283	Princeton Applied Research
Syringes, 60 mL	Becton Dickinson
UV transilluminator	VWR Scientific

Synthetic DNA; all sequences purchased from the Plant Biotechnology Institute

Ib-20 5`-AACTACTGGGCCATCGTGAC-$(CH_2)_6$ SS$(CH_2)_6$-OH 3`
IIb-20 5`-GTCACGATGGCCCAGTAGTT-3`
CTL-1 5`-HO$(CH_2)_6$SS$(CH_2)_6$GTGGCTAACTACGCATTCCACGACCAAATG-3`
CTL-2 5`-CATTTGGTCGTGGAATGCGTAGTTAGCCAC-3`

2.1.1 Preparation of Actinomycin D Solutions

Actinomycin D stock solutions were dissolved to 10 mg/mL in 95% ethanol. The stock solutions in ethanol were prepared fresh monthly and stored in the dark at 4 °C. Working solutions of between 1 pg/mL and 100 μg/mL were freshly prepared within five hours of completing a set of experiments. Working solutions were prepared by 1/100 dilution of the ethanolic actinomycin D solutions into 20 mM $NaClO_4$ and 20 mM Tris-ClO_4 pH 7.5.

2.1.2 Preparation of Redox Probe Solutions

The redox probe solution used in all experiments was a freshly prepared 4 mM solution of 1:1 $K_3[Fe(CN)_6]$:$K_4[Fe(CN)_6]$ dissolved in 20 mM $NaClO_4$ and 20 mM TrisClO_4 pH 7.5. Prior to use for experiments, argon gas was passed through the redox probe solution for 20 minutes in order to purge oxygen.

2.1.3 Preparation of Nucleic Acid Solutions

DNA duplexes were prepared by adding 10 nmol of disulphide-labeled DNA strands to 10 nmol of the complementary strands in 100 μL of 50 mM $NaClO_4$ and 50 mM Tris-ClO_4 pH 7.5 for 4 hours in the dark, at room temperature. The final concentration of dsDNA molecules was 0.1 mM. The complimentary oligonucleotide base sequences used were Ib-20 with IIb-20 and CTL-1 with CTL-2. Hybridization was confirmed by an ethidium fluorescence assay as described in Morgan *et al.*, 1979. Briefly, roughly 1 μg of DNA was added to 2.0 mL of 1.0 mM EDTA, 0.5 μg/mL Ethidium Bromide, and 10 mM TrisHCl pH 8.0. The fluorescence at 600 nm of this solution following excitation at 525 nm was measured on a Hitachi-2500 fluorescence spectrophotometer.

2.1.4 Preparation of Protein Solutions

Stock solutions of me-BSA and BSA were prepared at 2 mg/mL in 20 mM $NaClO_4$ and 20 mM Tris-ClO_4 pH 7.5. Working solutions were diluted from the stock solution with 20 mM $NaClO_4$ and 20 mM Tris-ClO_4 pH 7.5 to concentrations between 1.0 μg/mL and 1.0 mg/mL.

Antibody solutions were diluted to 1 mg/mL in 20 mM $NaClO_4$ and 20 mM Tris-ClO_4 buffer pH 7.5 from stock solutions of between 0.25 and 6.1 mg/mL in phosphate buffered saline (140 mM NaCl, 10 mM PO_4^- pH 7.4, and 2.7 mM KCl). Working solutions were diluted from the stock solution with 20 mM $NaClO_4$ and 20 mM Tris-ClO_4 pH 7.5 to concentrations between 0.1 μg/mL and 1 mg/mL. All protein solutions were stored at -20 °C in the dark.

2.2 Methods

2.2.1 Preparation of Electrodes

Gold electrodes of 1.6 mm diameter were polished with alumina oxide for 10 minutes on a polishing pad until the gold surface was smooth and unscratched. Surface smoothness was verified using a microscope under bright light. Deionized water from a Millipore Q system was used to wet the polishing pad during the cleaning process.

After being polished with alumina oxide, the electrodes were electrochemically treated by cycling from a potential of –0.2 to 1.6 V versus Ag/AgCl in 0.5 M H_2SO_4 solution until a stable gold oxidation peak at 1.1 V versus Ag/AgCl was obtained. In some cases, instead of cycling in 0.5 mM H_2SO_4, the electrodes were placed in a 3:1 mixture of H_2SO_4 and 30% H_2O_2 for 5 minutes. Following either chemical treatment, Millipore water was used to thoroughly rinse the electrodes before incubation with dsDNA. Prior to any further use of the electrodes, the impedance of the bare gold surface was measured with the method described below in section 2.2.3.

2.2.2 Preparation of Monolayers

2.2.2.1 Immobilization of DNA

The freshly-prepared gold electrodes were incubated with 5 μL of 0.1 mM duplex DNA solution for 5 days at room temperature. The electrodes were then rinsed thoroughly with 20 mM $NaClO_4$ and 20 mM Tris-ClO_4 pH 7.5 and mounted in an electrochemical cell containing a freshly prepared redox probe solution. Unless otherwise specified, all dsDNA monolayers used in the experiments were composed of 30mers.

2.2.2.2 Preparation of Mixed Monolayers

The freshly-prepared gold electrodes were incubated with 5 μL of 0.1 mM duplex DNA solution for 5 days at room temperature. The electrodes were then rinsed thoroughly with 20 mM $NaClO_4$ and 20 mM Tris-ClO_4 pH 7.5 and incubated with 5 μL of 0.1 mM butanethiol solution for 2 hours at room temperature. Following incubation with butanethiol,

the electrodes were rinsed thoroughly with 20 mM $NaClO_4$ and 20 mM Tris-ClO_4 pH 7.5 and mounted in an electrochemical cell containing freshly-prepared redox probe solution.

2.2.3 Electrochemical Measurements

All electrochemical measurements were performed at room temperature with a Princeton Applied Research model 283 potentiostat. The electrochemical cell used in all measurements consisted of the working electrode with or without an immobilized monolayer, a platinum wire counter electrode, and an Ag/AgCl reference electrode. The reference electrode was isolated from the cell by placing it in a saturated solution of KNO_3 (~3.5 M). All three electrodes were placed in a glass container with redox probe solution and connected to the potentiostat. Impedance was measured at the potential of 250 mV versus Ag/AgCl. All impedance data were analyzed and fitted to a Randles circuit or to a modified Randles circuit using ZSimpWin v. 2.00 software (Princeton Applied Research). The modified Randles circuit includes all of the components shown in figure 3 of section 1.1.3 and is fit to $R_s(C_{DL}(R_{CT}W))$. In contrast, the Randles circuit lacks the W component of the circuit shown in figure 3 and is fit to $R_s(C_{DL}R_{CT})$.

The impedance of a working electrode without an immobilized monolayer was measured following preparation of the electrode surface as described in section 2.2.1. The impedance was then measured on the same working electrode following preparation of the immobilized monolayer as described in section 2.2.2. Following measurement of the monolayer impedance the monolayer was exposed to solutions of polyamine, protein, or actinomycin D by placing a 5 μL drop of reagent solution on the surface of the working electrode and incubating for 30 minutes at room temperature. The electrode was then immediately submerged into the redox probe solution and the impedance measurements made. When assays were carried out with solutions of Hed 10, the dsDNA was in some cases denatured prior to exposure to Hed 10 by exposure of the dsDNA monolayer to 10 mM NaOH for 10 minutes at 60 ºC.

The impedance values observed in all experiments are expressed as R_{CT} (Ω). The R_{CT} observed following formation of the monolayer is the R_{CT} of the monolayer. However, all R_{CT} values observed following exposure of a monolayer to reagents are expressed as ΔR_{CT} rather than as R_{CT} in order to account for the contribution of the dsDNA monolayer to the R_{CT} of the dsDNA monolayer bound to reagent. Thus, all values of ΔR_{CT} expressed following exposure of the monolayer to reagents are the difference between the R_{CT} value observed following

exposure of the monolayer to polyamine, protein, or actinomycin D and the R_{CT} value observed following formation of the monolayer.

The percent ΔR_{CT} following exposure of the monolayer to polyamine, protein, or actinomycin D was calculated in order to normalize the ΔR_{CT} following exposure of the monolayer to any of these molecules with the R_{CT} observed following monolayer formation. The following equation was used to calculate percent ΔR_{CT}, where ΔR_{CT}^{Single} is the observed ΔR_{CT} in ohms following exposure of the monolayer to polyamine, protein, or actinomycin D, $R_{CT}^{Monolayer}$ is the R_{CT} observed following formation of the dsDNA monolayer in the same experiment (or in some experiments the remaining R_{CT} following denaturation of the dsDNA monolayer with NaOH), $\%\Delta R_{CT}^{Single}$ is the percent ΔR_{CT} for one experiment:

$$\frac{\Delta R_{CT}^{\ Single}}{R_{CT}^{\ Monolayer}} = \%\Delta R_{CT}^{\ Single} \qquad (2.1)$$

The $\%\Delta R_{CT}^{Single}$ values were then averaged and the standard deviations were calculated based on those averages to arrive at the values expressed below in sections 3.4 to 3.6.

2.2.4 Band Shift Experiments

Agarose solutions were prepared to 1.5 % in Tris-acetate-ethylenediaminetetraacetic acid (TAE) buffer (1.0 mM ethylenediaminetetraacetic acid, 40 mM Tris-acetate pH 8.0) and heated to allow complete dissolution of the agarose. This solution was then poured into a gel mould with a comb to create a gel with eleven wells. A solution of 100 µg/mL pT463-I and was prepared in 20 mM $NaClO_4$ and 20 mM Tris-ClO_4 pH 7.5. Five µL of pT463-I solution were mixed with 5 µL of either 87 µg/mL Jel 72 or 36 µg/mL Jel 274 in phosphate buffered saline and the resulting mixture was in turn mixed with 2 µL of loading buffer (10% (v/v) glycerol, 0.25% (w/v) bromophenol blue, 0.4 M Tris-HCl pH 8.8) following 30 minutes of incubation. A five µL aliquot of pT463-I was also mixed with a five µL aliquot of phosphate buffered saline without antibody as a control and then combined with 2 µL of loading buffer. Five µL of kilobase DNA ladder were also mixed with 2 µL of loading buffer. The solutions were incubated in high relative humidity for 30 minutes to allow the antibodies and the DNA to interact without dehydrating the small quantities of solution. These solutions were then loaded into the wells of the gel while the gel was immersed in TAE buffer in the gel electrophoresis apparatus. The gel electrophoresis apparatus was then connected to its power supply and 80 V of current was run through the gel for 2.5 hours. After being exposed to the

current, the gel was removed and placed in a 0.5 μg/mL (roughly 1.3 μM) solution of ethidium bromide in ddH_2O for 30 minutes. Following this incubation, the gel was placed on the UV transilluminator and visualized at 305 nm and a picture was taken with a Polaroid gel camera with 15 seconds of exposure.

3.0 Results

3.1 Preparation and Cleaning of Gold Surfaces

The R_{CT} values observed for bare electrodes were typically between 1,500 Ω and 3,000 Ω. These R_{CT} values are in agreement with the literature as discussed in section 1.1.2. A representative impedance plot for a bare gold electrode is shown below in figure 12. The semicircular portion of the graph indicates the impedance due to the presence of a kinetic process arising from any imperfections present in the gold surface, as well as the small resistance provided by the gold itself. The semicircular portion does not begin at the Z_{re} origin because there is a significant contribution of R_s to the impedance. The linear portion is the diffusion limited transmission of signal through the redox probe solution. This plot is based on the modified Randles circuit described in section 1.1.3, with both kinetic- and diffusion-based (R_{CT} and W, respectively) elements determining the impedance of the gold surface. However, since the properties of the monolayers are the focus of this study, R_{CT}, which is a measure of the kinetic resistance to charge transfer due to the properties of the gold surface (and any molecules absorbed thereon), is an appropriate datum to observe in the following sections 3.3 to 3.7.

3.2 Formation of dsDNA Monolayers

The R_{CT} values obtained following formation of dsDNA monolayer were on average 235,000 ± 110,000 Ω, which is a standard deviation of 47%. An impedance plot for a representative dsDNA monolayer is shown below in figure 13. These data were interpreted based on a Randles circuit as described in section 1.1.3. The semicircular shape of the graph indicates that the impedance is being governed by the R_{CT} arising from the properties of the monolayer and that the diffusion controlled W impedance is not contributing in any significant way to the impedance of the cell. The lack of effect W has on determining the impedance of the system is illustrated by the lack of a straight line at the second intercept with the Z_{re} axis. Thus, the increase in impedance following formation of a dsDNA monolayer

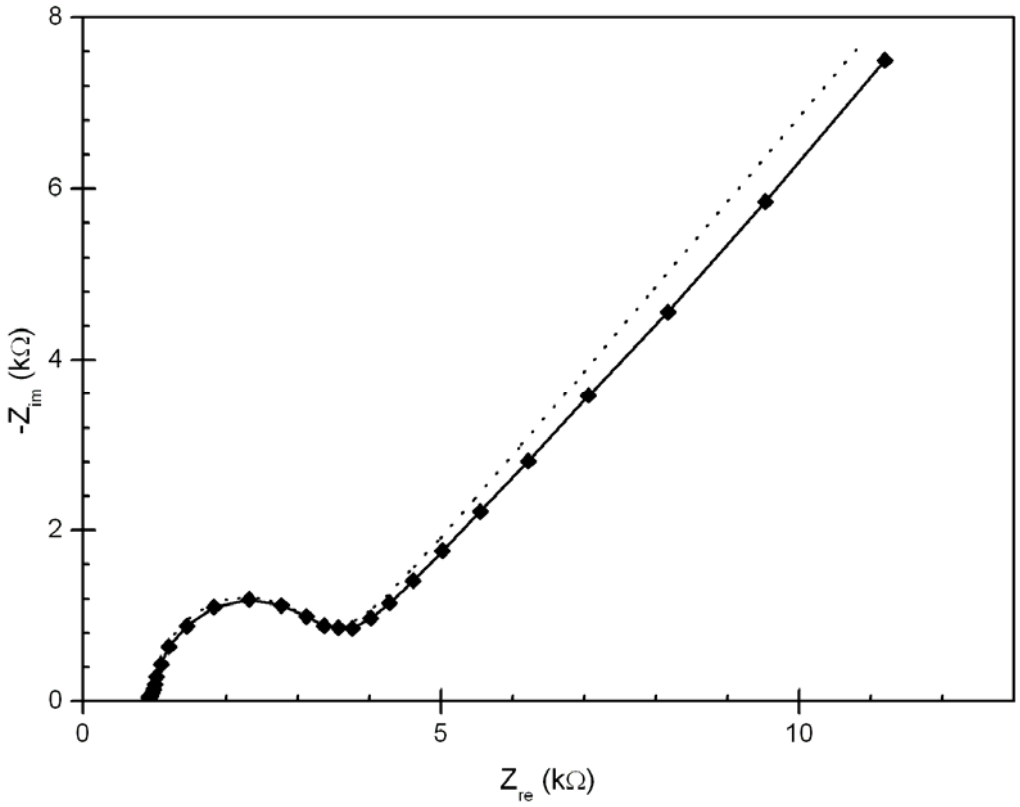

Figure 12: Impedance plot of a bare gold electrode. The R_{CT} is 2,745 Ω. The dashed line indicates a modified Randles circuit fit.

.

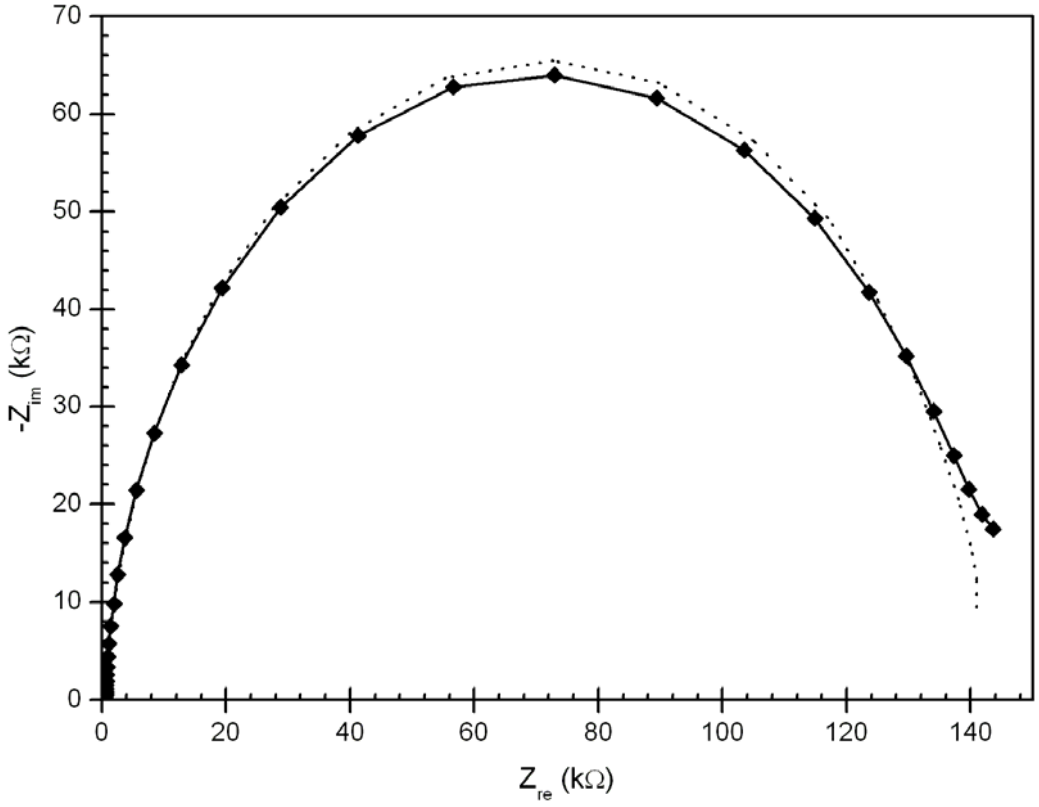

Figure 13: Impedance plot of an electrode with a DNA monolayer. The R_{CT} is 143,000 Ω. The dashed line represents a Randles circuit fit.

is due to the properties of the monolayer and not due to any change in the properties of the electrolyte solution, as expected.

The R_{CT} of a dsDNA monolayer was not constant between experiments. To improve the reproducibility of the magnitude of the R_{CT} observed following monolayer formation, the number of days of incubation for monolayer formation was varied and the effect of the duration of the incubation on the reproducibility of the monolayers was assessed. These experiments did not show any improved reproducibility in the R_{CT} of the monolayer when allowed to incubate for periods longer than five days, although the monolayers that were formed over a period shorter than five days were less reproducible than those formed for five days or more. In addition, the R_{CT} of a dsDNA monolayer formed over a period of less than five days was lower than those formed for five days or more, with a plateau being reached after five days of incubation. A representative experiment is shown below in figure 14.

Further attempts were made to improve the reproducibility of the R_{CT} observed following dsDNA monolayer formation by applying a two minute positive pulse of 450 mV to the electrode during monolayer formation. This produced a dsDNA monolayer with an acceptable R_{CT} in a very short period of time, but the monolayers were extremely unstable and would largely disappear following exposure to reagents, as shown below in figure 15. Figure 15 demonstrates that following exposure to spermine, the R_{CT} of the monolayer dropped by a much larger degree than that observed following exposure of other dsDNA monolayers to spermine. In addition to the larger drop, the shape of the impedance plot was drastically altered when compared to impedance plots of other monolayers following exposure to spermine. The tail of the impedance plot of these dsDNA monolayers following exposure to spermine indicated that the Warburg diffusion is playing a much greater role than in more stable monolayers. The presence of Warburg diffusion indicated that the dsDNA monolayer is playing a much-reduced role in determining the electrochemical properties of the cell. Thus, there is much less DNA present on the gold as compared to electrochemical cells with dsDNA monolayers formed by slow incubation without a positive current. The results of experiments on the exposure of spermine to more stable dsDNA monolayers are shown below in section 3.4.2.

To account for the large standard deviation in the R_{CT} of monolayer formation, all data for binding events following DNA monolayer formation were calculated as a percentage of the R_{CT} for the dsDNA monolayer that the individual experiment was performed with as described in section 2.2.3. Averages of ΔR_{CT} values following binding of reagents described below in sections 3.3, 3.4, and 3.5, respectively, were then calculated following expression of

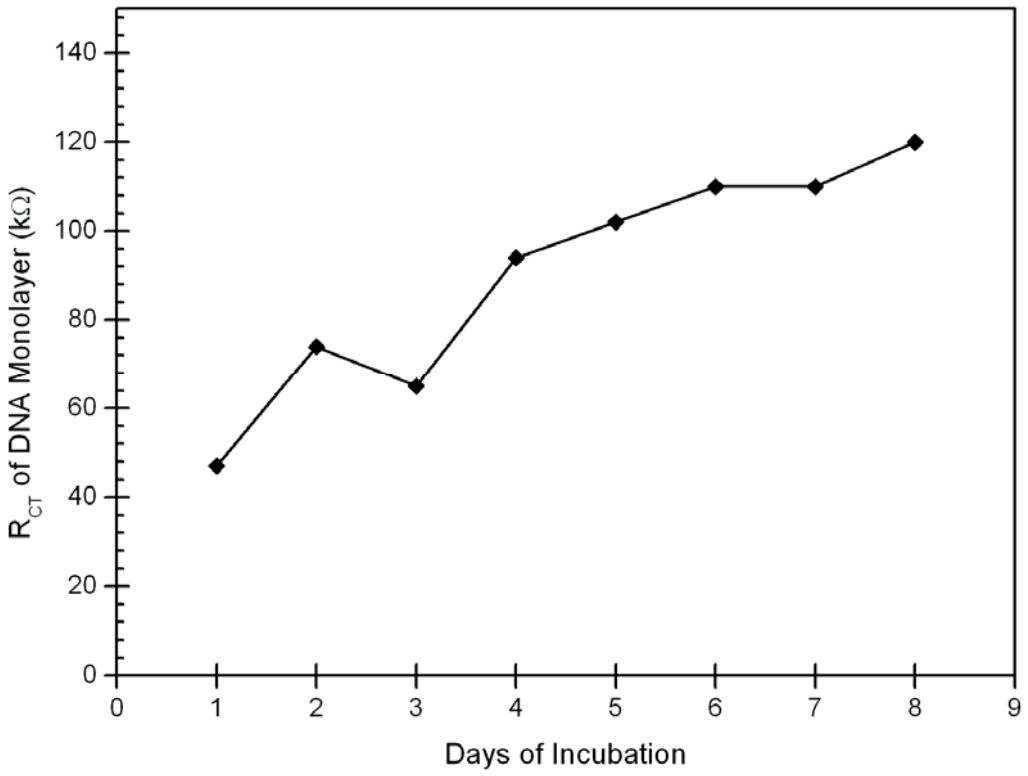

Figure 14: R_{CT} values obtained following formation of dsDNA monolayers for between one and eight days. The plateau values are attained beginning with day four.

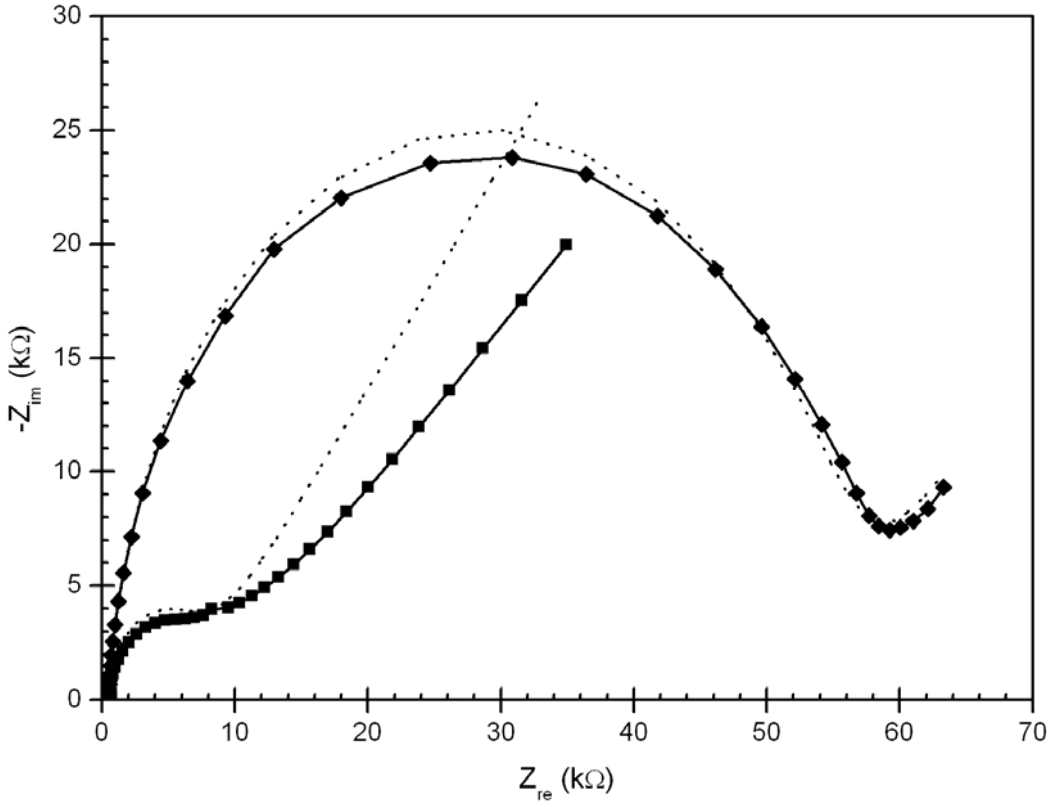

Figure 15: Impedance measurement of a pulse-generated dsDNA monolayer before (diamonds) and after (squares) incubation with 0.5 mM spermine. The ΔR_{CT} value following exposure to spermine was -50,000 Ω or -83%. The dashed lines represent a modified Randles circuit fit.

these values as percentages of the R_{CT} following formation of the dsDNA. This method of averaging substantially lowered the standard deviation in the ΔR_{CT} values.

3.2.1 Dilution of DNA Monolayers with Butanethiol

Exposure of the dsDNA monolayer to butanethiol prior to incubation with proteins was attempted in order to allow antibodies better access to DNA. This was based on the theory that butanethiol spreads out the DNA molecules allowing the antibodies better access to the DNA. Following exposure of the dsDNA monolayer to butanethiol, ΔR_{CT} of -11 ± 8 % and -32 ± 12 % were observed for the 20mer and for the 30mer, respectively. Representative data obtained in experiments testing the response of the DNA monolayer to butanethiol are shown in figure 16. In this experiment there was a ΔR_{CT} of approximately -33 % upon exposure of a 30mer dsDNA monolayer to butanethiol. The reduction in R_{CT} was expected because the negatively-charged DNA molecules were being replaced by much smaller and non-charged butanethiol molecules, thus allowing the negatively-charged redox probe better access to the surface because steric and electronic impediments to transfer that make up part of the R_{CT} were reduced relative to a monolayer composed exclusively of DNA.

3.3 Exposure of DNA Monolayers to Buffer

In order to verify that the buffer itself and/or the process of adding a drop of liquid to the electrode was not causing a change in the R_{CT} of the monolayer, the dsDNA monolayer was exposed to buffer lacking any additional reagents and there was no significant ΔR_{CT} observed. A representative experiment is shown below in figure 17. Similar results were observed with ssDNA monolayers (data not shown). Multiple repeats of this experiment showed exposure of the DNA monolayer to buffer results in a ΔR_{CT} of -13.5 % ± 8.4 %. Thus, the detection threshold for all experiments described below is a ΔR_{CT} of -13.5 % ± 8.4 %; any changes smaller than these are not significant. Conversely, any results of a ΔR_{CT} of greater than -13.5 % ± 8.4 % are significant and due to interaction of the relevant molecules with the DNA monolayer.

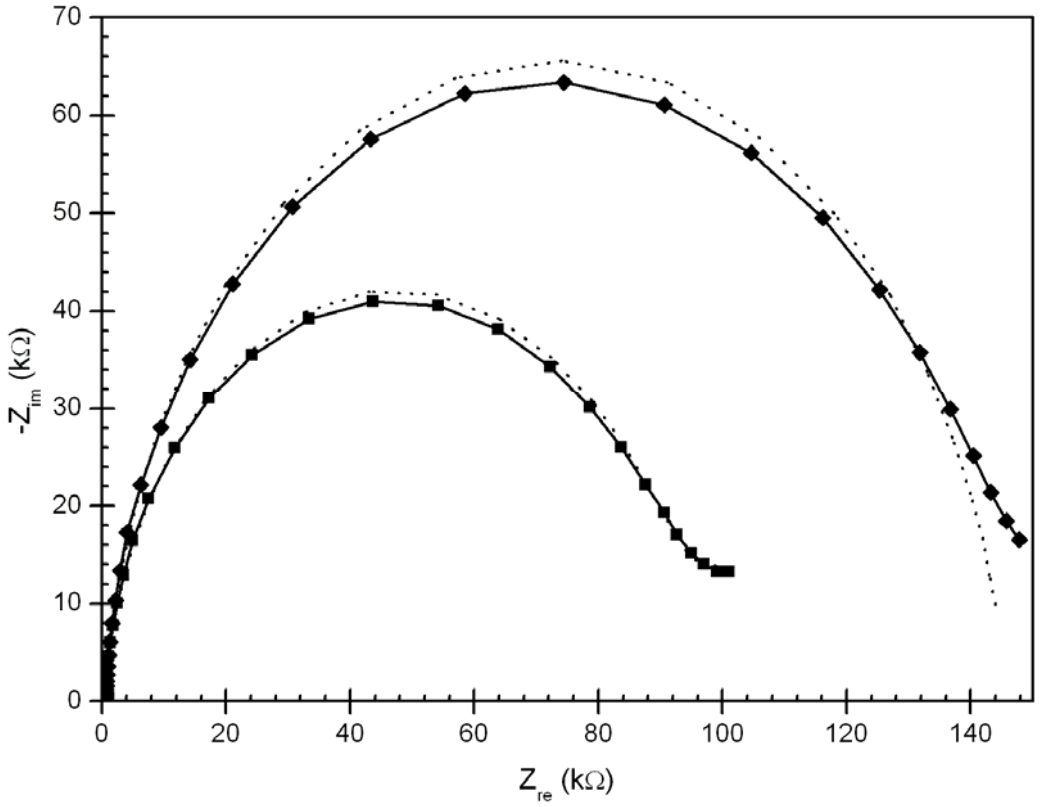

Figure 16: The DNA monolayer before (diamonds) and following (squares) incubation with 0.1 mM butanethiol. The ΔR_{CT} following exposure to butanethiol is -48,000 Ω or -33 %. The dashed line for the DNA monolayer prior to exposure to butanethiol represents a Randles circuit fit. The dashed line for the DNA monolayer following exposure to butanethiol represents a modified Randles circuit fit.

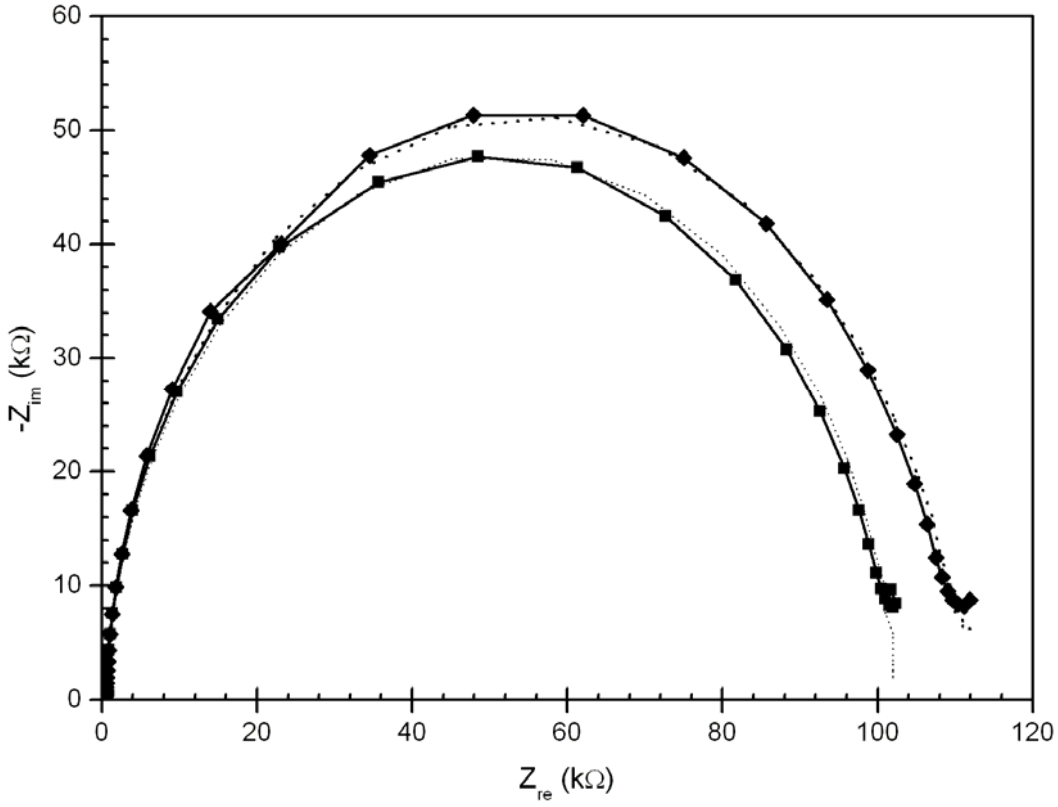

Figure 17: Impedance measurement of the DNA monolayer before (diamonds) and after (squares) incubation with 20 mM $NaClO_4$ and 20 mM $TrisClO_4$ pH 7.5. A ΔR_{CT} of -8,000 Ω, or -7.2%, was observed following incubation of the monolayer with buffer. The dashed line for the DNA monolayer prior to exposure to buffer represents a modified Randles circuit fit. The dashed line for the DNA monolayer following exposure to buffer represents a Randles circuit fit.

3.4 Binding of Polycations to DNA Monolayers

3.4.1 Polylysine

As indicated by figure 18, the ΔR_{CT} of the 20mer dsDNA monolayer following exposure to polylysine is negative. The implications of the negative ΔR_{CT} will be discussed in section 4.2. The data in figure 18 was obtained with an equivalent concentration of 6.8 nM (calculated as lysine monomers).

3.4.2 Spermine

The ΔR_{CT} observed following binding of spermine to a dsDNA monolayer was negative. The spermine concentrations used ranged from 0.05 nM to 1 mM. The ΔR_{CT} following exposure of a DNA monolayer to 5.0 μM spermine is shown below in figure 19. A plot of $\%\Delta R_{CT}$ at various concentrations of spermine is shown in figure 20. Given the threshold ΔR_{CT} of -13.5 % ± 8.4 % for a significant change as detailed in section 3.3, the data points between 0.05 nM and 0.5 μM do not show a significant ΔR_{CT}. The lower limit of spermine detection is thus around 0.5 μM. At concentrations above 0.5 μM, beginning with 5.0 μM, spermine causes a decrease in the R_{CT} of the dsDNA monolayer, the implications of which are discussed below in section 4.2. The sensitivity for spermine is thus higher than for polylysine since the polylysine experiments showed detection at concentrations roughly one hundred times more dilute than the lowest spermine concentration that showed a significant signal.

3.5 Binding of Actinomycin D to DNA Monolayers

No significant signal was observed following exposure of between 1 pg/mL and 100 μg/mL of actinomycin D to the dsDNA monolayer as shown below in figure 21. As indicated in figure 21, none of the assayed concentrations were significantly different than the control. In this case, the control was exposure of the dsDNA monolayer to a 1 % solution of ethanol in buffer.

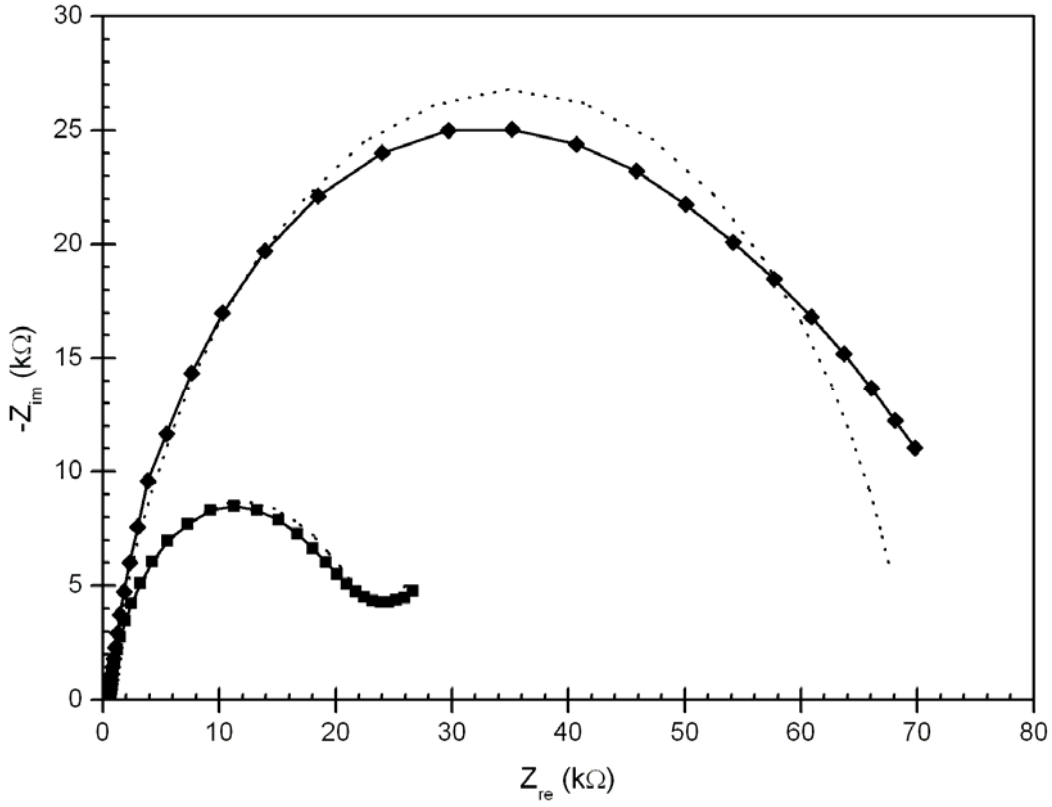

Figure 18: Impedance plot of a DNA monolayer before (diamonds) and after (squares) incubation in the presence of 6.8 nM (calculated as lysine monomers) polylysine. The ΔR_{CT} following polylysine binding was -47,000 Ω or -67 %. The dashed line for the DNA monolayer prior to exposure to polylysine represents a Randles circuit fit. The dashed line for the DNA monolayer following exposure to polylysine represents a modified Randles circuit fit.

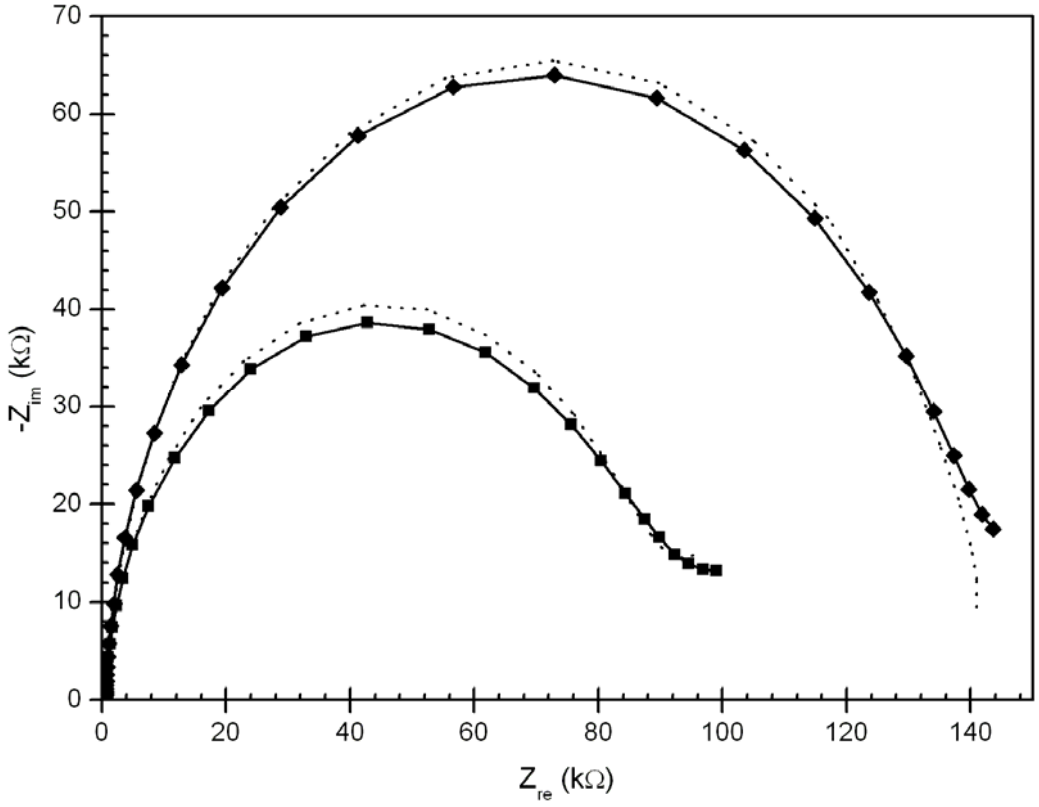

Figure 19: Impedance measurement of the DNA monolayer before (diamonds) and after (squares) incubation with 5.0 μM spermine. The ΔR_{CT} following spermine binding was -44,000 Ω or -31 %. The dashed line for the DNA monolayer prior to exposure to spermine represents a Randles circuit fit. The dashed line for the DNA monolayer following exposure to spermine represents a modified Randles circuit fit.

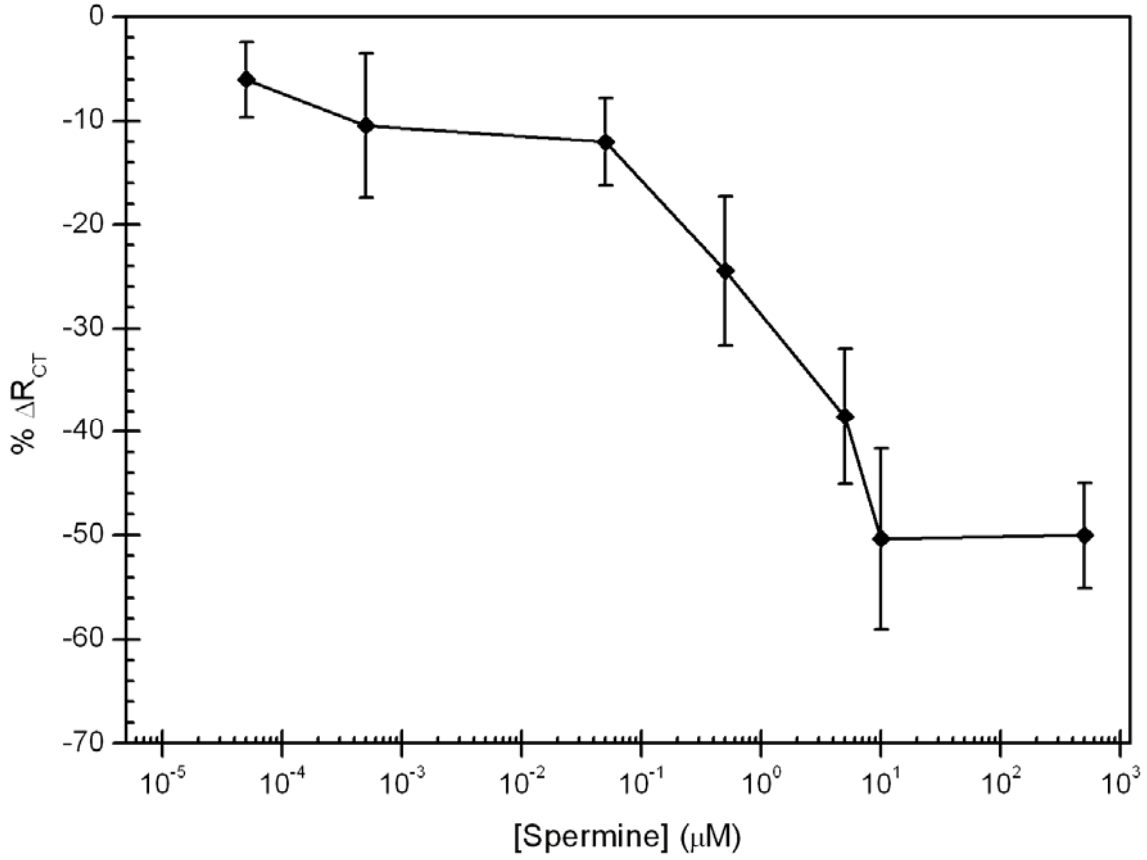

Figure 20: Percent ΔR_{CT} values observed following exposure of the dsDNA monolayer to spermine. The error bars are the standard deviation for the experiments.

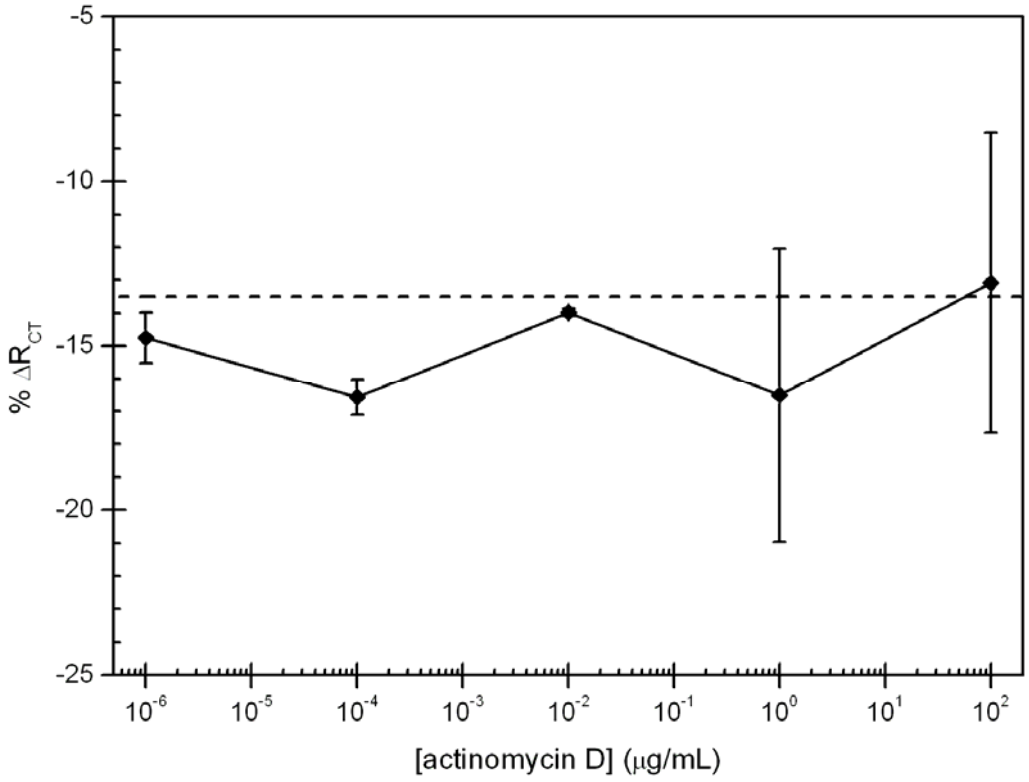

Figure 21: Percent ΔR_{CT} values observed following exposure of a dsDNA monolayer to varying concentrations of actinomycin D. The percent ΔR_{CT} values observed following exposure of a dsDNA monolayer to 1 % ethanol in buffer is shown as a dashed line. The error bars are the standard deviation for the experiments.

3.6 Binding of Proteins to DNA Monolayers

3.6.1 Methylated Bovine Serum Albumin

To ascertain the effect of non-specific protein-DNA interactions mediated through the phosphate backbone and positive charges on proteins, me-BSA and BSA were exposed to the 20mer dsDNA monolayer at concentrations between 1.0 μg/mL and 1.0 mg/mL. Concentrations of 50 μg/mL or higher of me-BSA showed a large positive ΔR_{CT}. The ΔR_{CT} observed as a result of exposure of the DNA monolayer to 500 μg/mL me-BSA is shown in figure 22. Exposure at all concentrations resulted in a logarithmic sigmoid concentration-dependent curve, as illustrated in figure 23. Control experiments with BSA over the same concentration range only showed a significant increase in the R_{CT} at concentrations of 1 mg/mL, and this increase was still only half of that caused by me-BSA at the same concentration. The results of exposing the DNA monolayer to 100 μg/mL BSA is shown below in figure 24, while a plot of exposure of the DNA monolayer to all assayed concentrations of BSA is shown in figure 25. As apparent from figures 22 and 24, me-BSA causes a much larger ΔR_{CT} than BSA when either protein is exposed to the dsDNA monolayer. Figures 23 and 25 show that although 1 mg/mL BSA does cause a significant ΔR_{CT}, high concentrations of me-BSA cause a much larger ΔR_{CT} than high concentrations of BSA exposed to the dsDNA monolayer. There is also a more pronounced dependence of the observed ΔR_{CT} on the concentration of protein exposed to the dsDNA monolayer with me-BSA than with BSA.

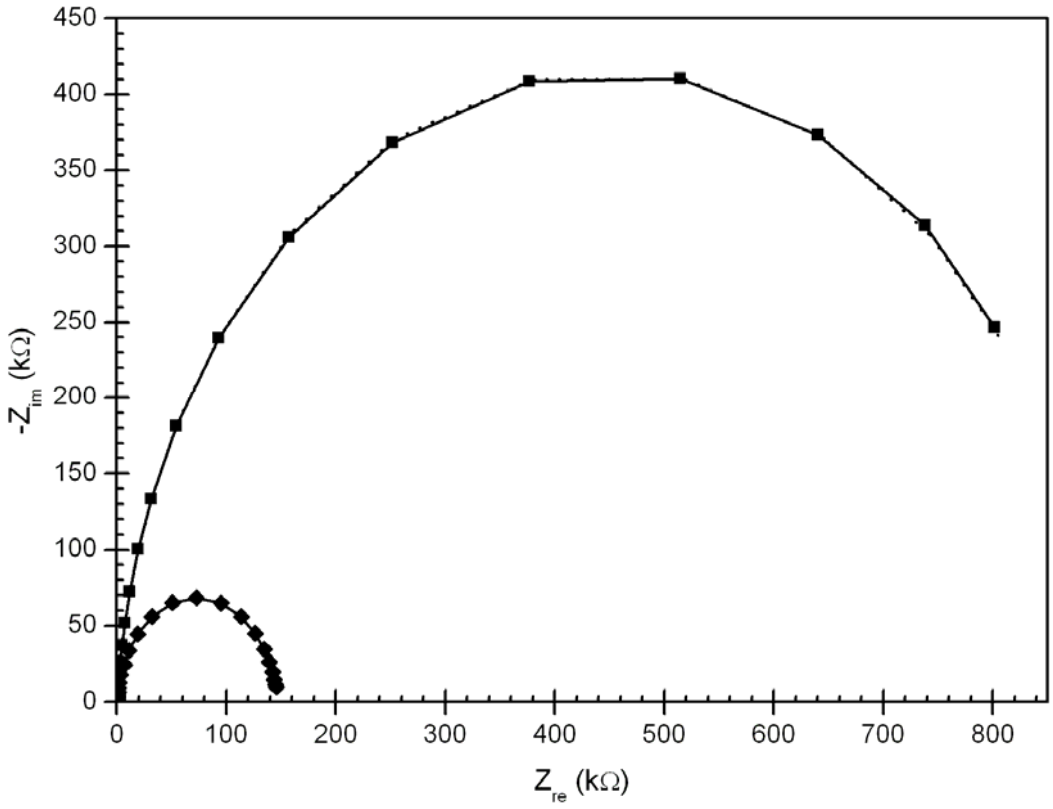

Figure 22: Impedance measurement of the DNA monolayer before (diamonds) and after (squares) incubation with 500 μg/mL of me-BSA. The difference in R_{CT} values is + 655,000 Ω or 452 %. The dashed lines represent a Randles circuit fit.

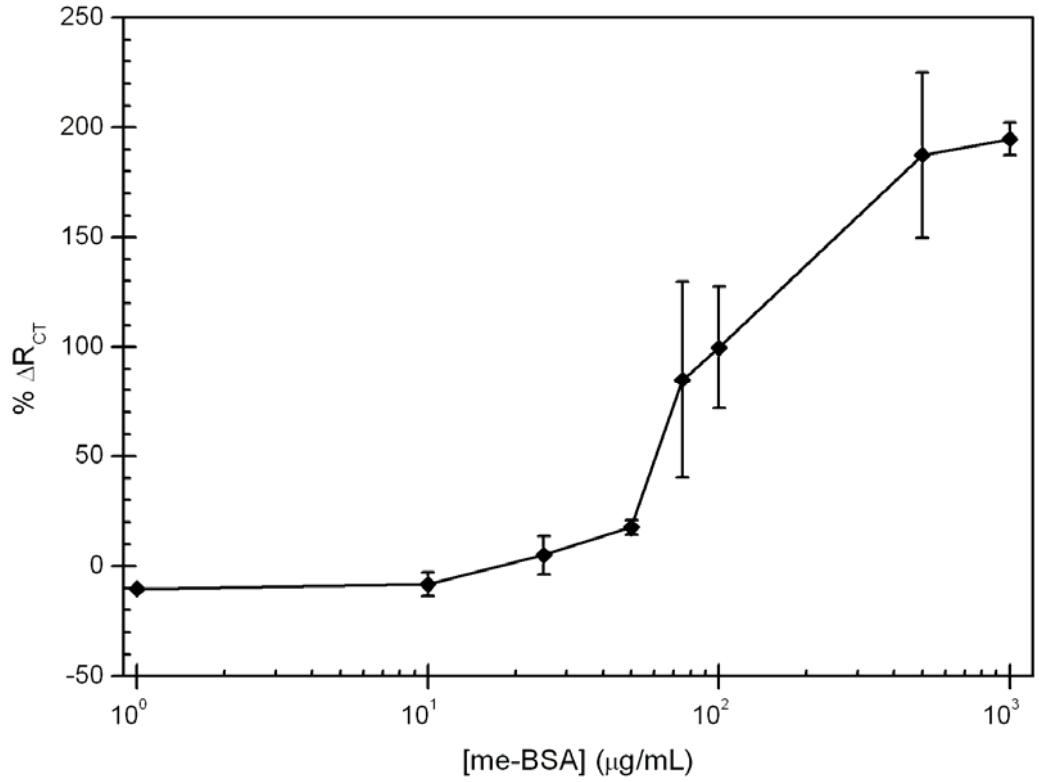

Figure 23: Plot of the ΔR_{CT} values obtained following exposure of the DNA monolayer to varying concentrations of me-BSA. The relationship is sigmoidal when me-BSA concentration is expressed logarithmically. The error bars are the standard deviation for the experiments.

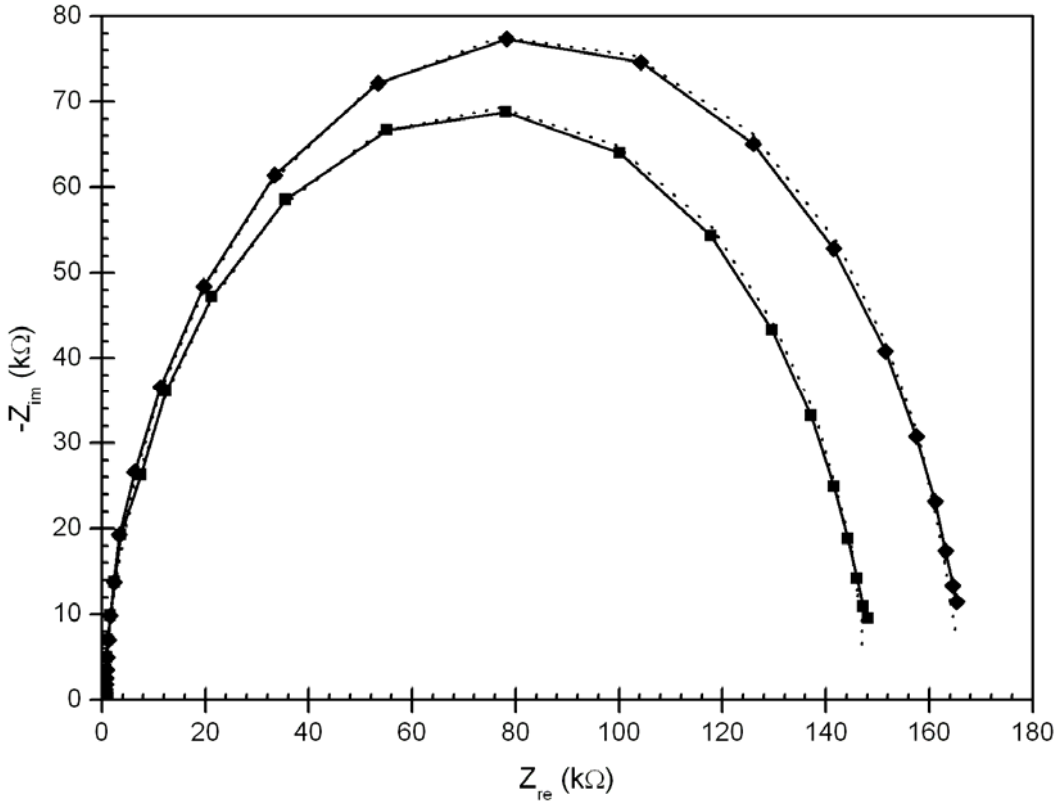

Figure 24: Impedance measurement of the DNA monolayer before (diamonds) and after (squares) incubation with 100 μg/mL of BSA. The difference in R_{CT} values is - 17,000 Ω or - 10.3 %. The dashed lines represent a Randles circuit fit.

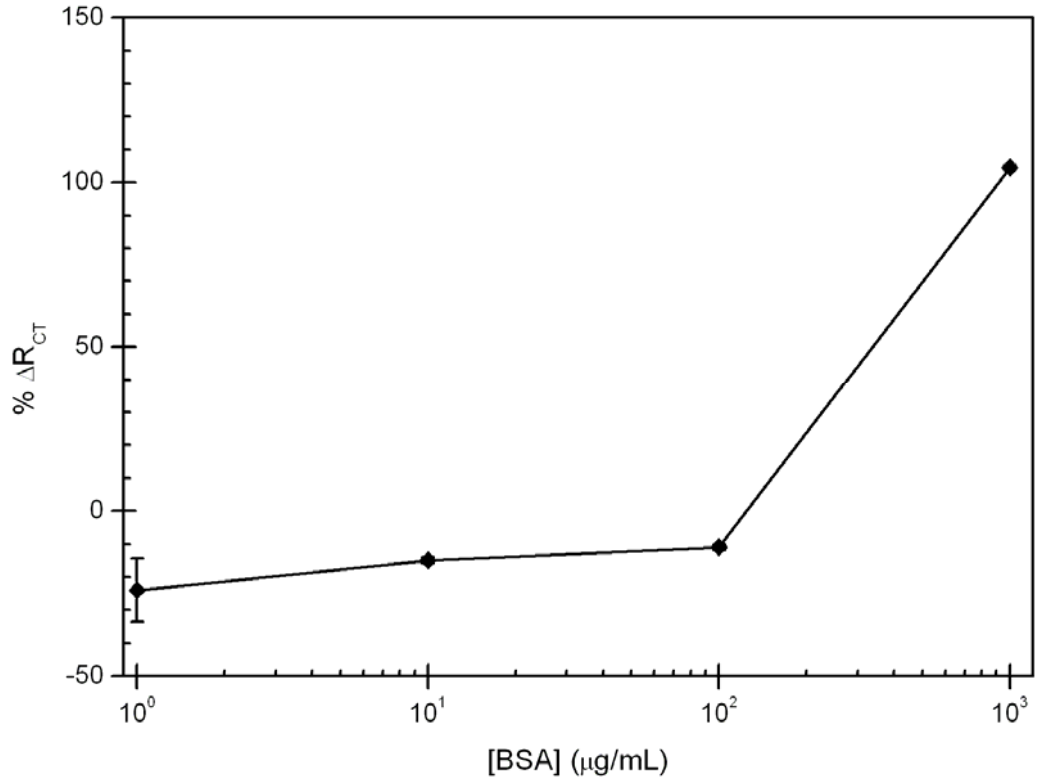

Figure 25: Plot of the ΔR_{CT} values obtained following exposure of the DNA monolayer to varying concentrations of BSA. There is no sigmoidal relationship as observed with me-BSA. The error bars are the standard deviation for the experiments.

3.6.2 Jel 72 and Jel 274

No significant binding of either Jel 72 or Jel 274 was observed under any conditions assayed. No signals that were outside of the baseline range defined in section 3.3 were observed regardless of variables that were changed in the experiments. The variables that were modulated in the experiments were the antibody used, the length of the DNA, the presence or absence of butanethiol dilution in the monolayer, and the concentration of antibody used. None of these variables had any significant impact on the % ΔR_{CT} observed when the variables were altered.

When 13 μg/mL of antibody was exposed to a 20mer diluted with butanethiol, the observed % ΔR_{CT} values were 6 ± 10% and -7 ± 7 % for Jel 72 and Jel 274, respectively. Thus, the particular antibody used had no significant impact on the % ΔR_{CT} values observed.

The effect of 33 μg/mL of Jel 72 was assayed with butanethiol-diluted monolayers composed of both the 20mer and the 30mer dsDNA sequences and no significant difference was seen between the two sets of experiments. Experiments with the 30mer showed a ΔR_{CT} of 7 ± 16%, while experiments with the 20mer showed a ΔR_{CT} of 3 ± 5%.

Similarly to the above two trends, the presence or absence of butanethiol dilution had no measurable impact on the observed % ΔR_{CT} values when a 30mer was exposed to 33 μg/mL of Jel 72. The experiments with butanethiol showed a ΔR_{CT} of 7 ± 16%, while experiments without butanethiol dilution showed a ΔR_{CT} of 3 ± 5%.

Finally, the concentration of antibody had a negligible impact on the observed % ΔR_{CT} values when a butanethiol-diluted 30mer was exposed to Jel 72. The results over a concentration range of 3 to 33 μg/mL of Jel 72 showed no substantial differences between different concentrations, as illustrated below by figure 26. Furthermore, when the results of all concentrations were averaged together, the % ΔR_{CT} was 5 ± 14 %. The relatively low value and standard deviation despite that different concentrations are being mixed was a strong indication that there is no significant difference between the results observed at different concentrations of Jel 72.

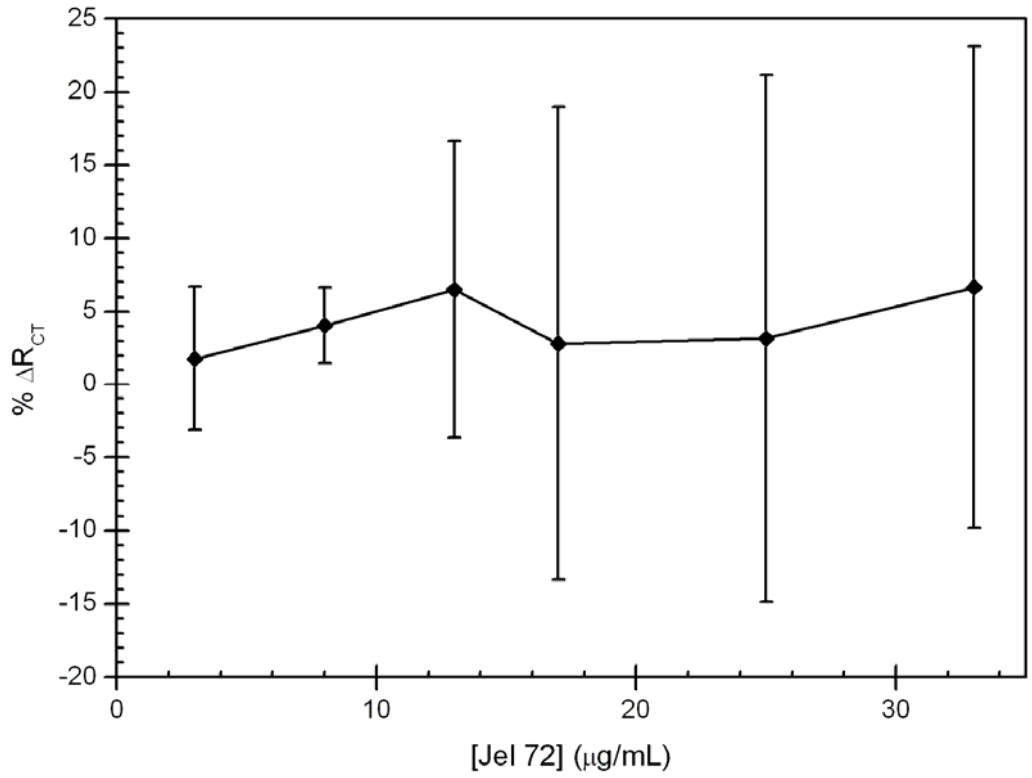

Figure 26: Plot of the percentage ΔR_{CT} values obtained following exposure of the 30mer dsDNA monolayer diluted by exposure to 0.1 mM mM butanethiol at all concentrations of Jel 72 assayed in this study. The error bars represent the standard deviation.

3.6.3 Hed 10

A representative plot showing exposure of 100 μg/mL Hed 10 to a ssDNA monolayer is shown below in figure 27. The results of experiments on exposure of Hed 10 to both dsDNA and ssDNA monolayers over a concentration range of 0.1 μg/mL to 1 mg/mL Hed 10 are summarized below in figure 28.

As shown in figure 28, Hed 10 caused a significant positive ΔR_{CT} following exposure of concentrations of at least 10 μg/mL Hed 10 to the ssDNA monolayer, with a maximum ΔR_{CT} of 103 ± 25 % at 1 mg/mL. In contrast, there was no significant ΔR_{CT} observed following exposure of Hed 10 to a monolayer of dsDNA. Even following exposure of the dsDNA monolayer to 1 mg/mL of Hed 10, the ΔR_{CT} was only 5 ± 8 %. The results in figure 27 at 100 μg/mL Hed 10 and the summary results in figure 28 together indicate that Hed 10 is not binding to dsDNA, but is binding to ssDNA and causes a significant ΔR_{CT} upon binding. These results are consistent with observations in previous work with Hed 10 which showed a high degree of specificity for ssDNA as compared to dsDNA. These results are also consistent with the results following exposure of the dsDNA monolayer to me-BSA, which suggests that binding of protein with the dsDNA monolayer increases the R_{CT} of the monolayer.

3.7 Band Shift Experiments

Agarose gel electrophoresis experiments showed binding between Jel 72 and the plasmid pT463-I, but a lack of binding between Jel 274 and pT463-I. The results of the band shift experiments are shown below in figure 29. When the plasmid pT463-I was run through the gel, two bands were visible. These bands likely correspond to different supercoiled conformations of the plasmid. Similarly, when the plasmid was run following incubation with Jel 274, the same bands were observed. Thus the presence of Jel 274 does not affect the mobility of the DNA in the gel which indicates that Jel 274 is likely not binding to the plasmid. In contrast, following incubation with Jel 72, the plasmid remained in the well and there was no DNA visible beyond the well. The results observed in the lane having Jel 72 and the plasmid are consistent with binding between the antibody and the plasmid since the increased molecular weight of the plasmid owing to binding would prevent the DNA from migrating through the gel at the rate it does in the absence of Jel 72.

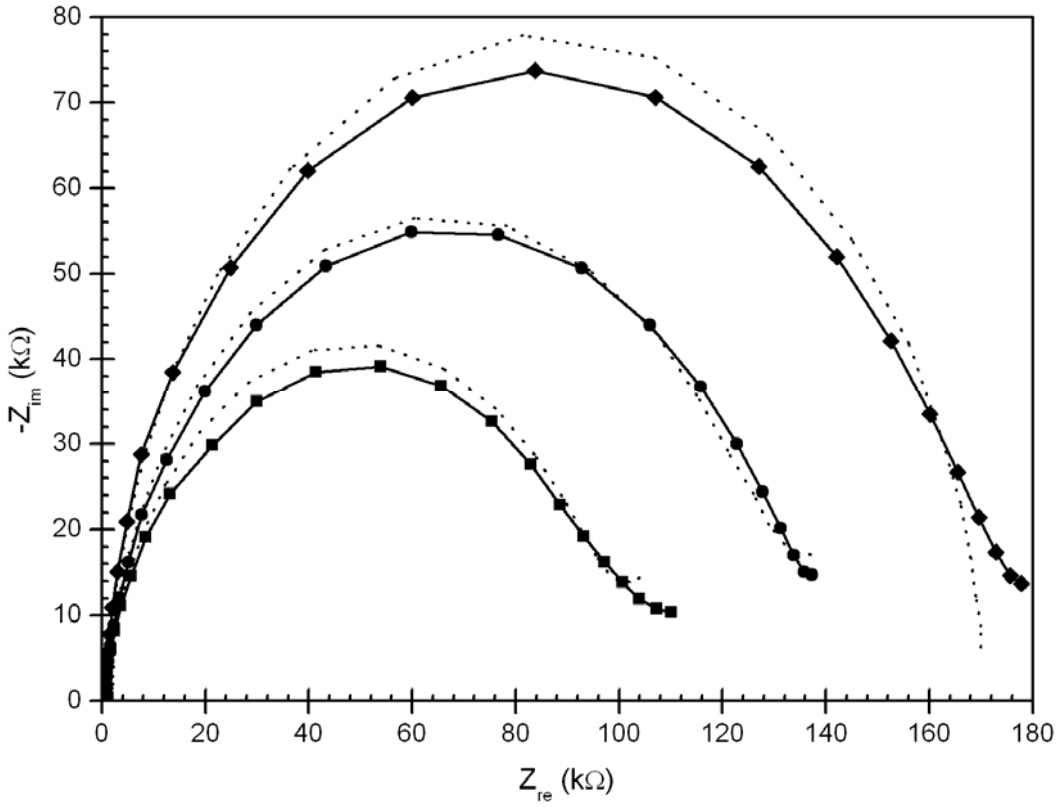

Figure 27: Impedance measurement of the DNA monolayer before (diamonds) and after (squares) denaturation and following incubation of the ssDNA monolayer with 100 μg/mL of Hed 10 (circles). The difference in R_{CT} values following exposure of the ssDNA monolayer to Hed 10 is + 27,000 Ω or 25 %. The dashed line for the DNA monolayer prior to denaturation represents a Randles circuit fit. The dashed lines for the DNA monolayer following denaturation and following exposure to Hed 10 represent a modified Randles circuit fit.

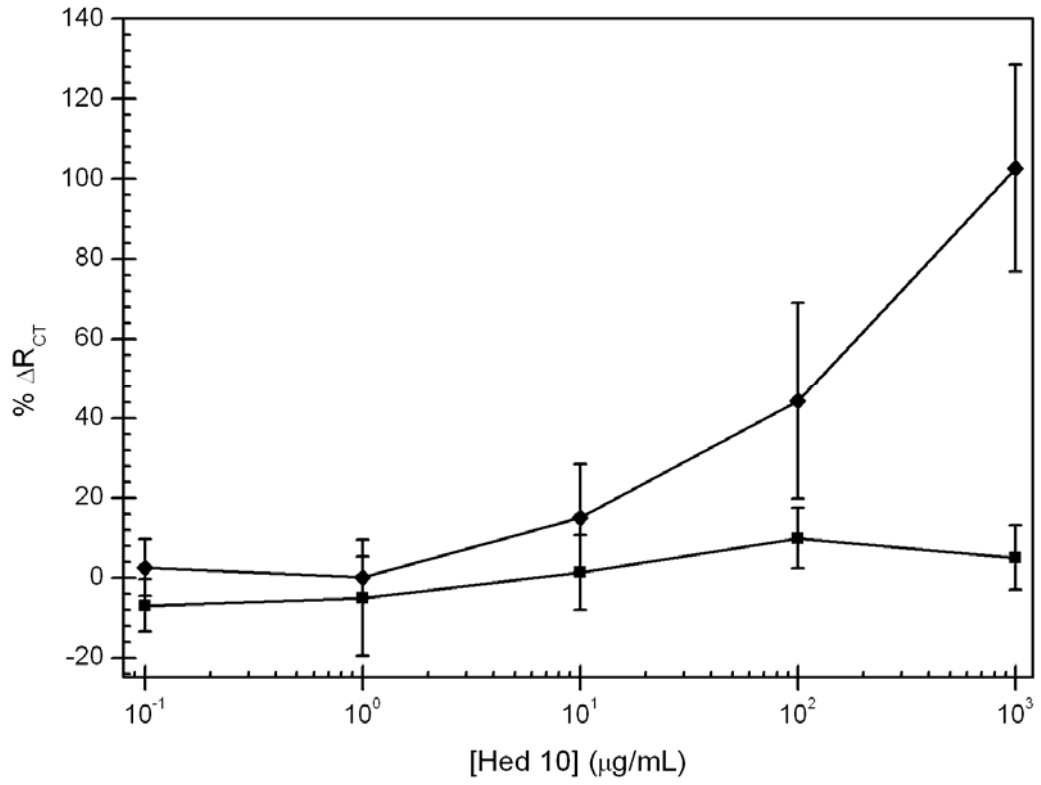

Figure 28: The percentage ΔR_{CT} values observed following exposure of various concentrations of Hed 10 monolayers of ssDNA (diamonds) and dsDNA (squares). The error bars are the standard deviation for the experiments.

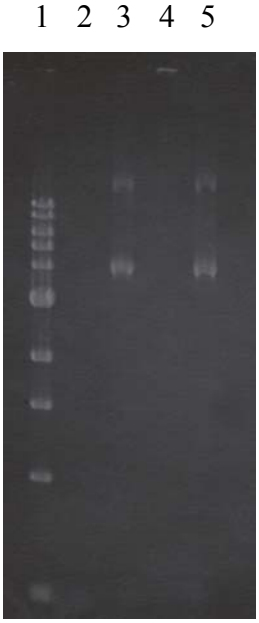

Figure 29: The results of the band-shift experiment with Jel 72. The lanes contain the following reagents by number: 1, Kilobase Molecular Weight Ladder; 2, (blank); 3, pT463-I; 4, pT463-I and 87 μg/mL Jel 72; 5, pT463-I and 36 μg/mL Jel 274. The lanes are positioned at the top of the figure and the positive pole of the current was at the bottom of the figure.

4.0 Discussion

4.1 Formation of Monolayers

Monolayers formed from 30mers had a higher R_{CT} than those formed from 20mers. If the monolayers formed from 30mers are less densely packed, it is likely they are presenting more binding sites than the monolayers formed from 20mers and that these binding sites are more accessible than those on the monolayers formed from 20mers. In light of this, all data discussed unless otherwise indicated are obtained with a 50 % GC 30mer of the sequence given in the materials and methods section.

In order to improve the reproducibility of the R_{CT} observed following formation of the dsDNA monolayer, a number of changes to the procedure were attempted. First, fresh electrodes, fresh solutions, and freshly-prepared dsDNA 30mers were used. Second, the number of days allowed for monolayer formation was varied between one and eight days. The incubations that were allowed to proceed for five days showed better results than those that were allowed to proceed for shorter periods. Third, applying a short positive pulse of 450 mV for two minutes during monolayer formation was attempted. The experimental conditions of the third method were materially similar to those of the other methods apart from the described short pulses. The first group of changes did not improve the reproducibility, while the last two changes attempted produced unstable monolayers. The monolayers formed in less than five days had smaller R_{CT} values than those formed for five days. The monolayers that were formed over a period of time greater than five days had greater R_{CT} values than those formed in five days, but the increase in R_{CT} was much less after the fourth day. Thus a five day incubation period was chosen because it was immediately after the last large daily increase in R_{CT} and appeared to be the beginning of the plateau. The results of these experiments are shown in figure 14. When the short pulses were applied, the dsDNA monolayers produced had smaller R_{CT} values than those obtained following incubation for five days by 69.5 %. Additionally, after incubation with 0.5 mM spermine, the dsDNA monolayers generated following short pulses showed a ΔR_{CT} of -68.3 ± 13.9 % compared with a with a ΔR_{CT} of -49.98% ± 7.2 % following exposure of the five-day dsDNA monolayer

to the same concentration of spermine. Additionally, the pulse-generated dsDNA monolayers had a long tail at the higher frequencies of Z_{re} following exposure to 0.5 mM spermine. Collectively, these results indicate an unstable monolayer, both because of the lower R_{CT} values of monolayer formation and because of the tail shown following incubation with spermine, which indicates a diffusion limited process compared to a kinetic process as expected with a full dsDNA monolayer. A representative experiment showing the effects of spermine addition to a pulse-generated monolayer is shown in figure 15.

4.1.1 Dilution of DNA Monolayers with Butanethiol

Upon exposure of the dsDNA monolayers to butanethiol, the R_{CT} of the monolayer decreased. This result is consistent with the DNA monolayer being diluted, allowing better access of the redox probe to the gold surface. There are three possible ways that the butanethiol is lowering the R_{CT} of the DNA monolayer. First, the butanethiol could be replacing dsDNA molecules with smaller molecules that have a lower steric hindrance. This is possible because the lowered steric hindrance would allow the redox probe to more easily pass to the gold surface without colliding with molecules of the monolayer. Second, by replacing dsDNA molecules with butanethiol molecules, the overall negative charge of the monolayer would be lowered since each dsDNA molecule has 40 or 60 negative charges (depending on whether the 20mer or 30mer was being used) on the phosphate backbones of both DNA strands. Thus, by replacing the dsDNA molecules with butanethiol molecules, the ionic repulsion between the redox probe and the monolayer would be lowered, which would facilitate access by the redox probe to the gold surface. Third, a combination of the above two effects could be producing the lowered R_{CT} of the monolayer following replacement of some dsDNA molecules with butanethiol molecules. All three of these possible explanations for the lowered R_{CT} following replacement of some dsDNA molecules with butanethiol molecules involve facilitating access by the redox probe to the gold surface; the only difference between the explanations is whether this facilitated access is due to lowered steric interference, lowered ionic repulsion, or both.

4.2 Binding of Polycations to DNA Monolayers

The ΔR_{CT} observed following exposure of both spermine and polylysine to the dsDNA monolayer is negative, indicating that the redox probe interacts more easily with the gold

surface. Both spermine and polylysine have multiple positive charges at pH 7.5, which are likely binding to the negatively-charged phosphate backbone of the dsDNA molecules in the monolayer. By binding to the negatively-charged phosphate backbone through ionic interactions, both polyamines are completely or partially neutralizing the negative charges on the phosphate backbone. Thus, the lowered R_{CT} observed following incubation of polyamines with the dsDNA monolayer could be due to a facilitated interaction between the gold surface and the redox probe because of lowered charge repulsion between the negatively-charged redox probe and the partially neutralized phosphate backbones in the DNA monolayer.

The ΔR_{CT} observed following exposure of the dsDNA monolayer to increasing concentrations of spermine shows that higher concentrations of spermine cause a greater decrease in the R_{CT} of the monolayer. Additionally, the ΔR_{CT} reaches a plateau at 10 μM spermine, with concentrations as high as 500 μM having no additional effect. This particular concentration dependence is also consistent with spermine neutralizing the phosphate backbone of the DNA and consequently facilitating access to the gold surface by the negatively charged redox probe. It is likely that below 10 μM spermine, there is insufficient spermine present in the solution to saturate the phosphate backbone, neutralizing all of the negatively charged phosphates. Alternatively or in combination with maximum spermine binding, it is possible that at concentrations above 10 μM, other effects of the presence of spermine are beginning to offset the lowered negative charge of the dsDNA monolayer.

The plateau ΔR_{CT} observed at 10 μM spermine is 45 %, indicating that the R_{CT} of the dsDNA monolayer cannot be entirely eliminated by exposure to polyamines. If the lowered R_{CT} is due to charge neutralization of the phosphate backbones, it is likely that the remaining R_{CT} is present because of steric hindrance caused by the mere presence of the neutralized dsDNA molecules. The presence of the neutralized dsDNA molecules would lower the accessibility of the redox probe to the gold surface similarly to butanethiol, which has no charge when bound to the gold surface, but also increases the R_{CT} relative to the R_{CT} of bare gold.

The negative ΔR_{CT} observed following exposure of the monolayer to polylysine is also consistent with the above discussion in relation to spermine. Although polylysine is found to cause effective DNA condensation only under cooperative binding conditions, which are likely not present with only 20 mM $NaClO_4$ (Liu *et al.*, 2001), it is possible that the degree of condensation that is occurring in the conditions of this experiment are sufficient to remove some of the steric block presented by the DNA to the redox probe's ability to contact the gold surface. Additionally, even if no condensation is occurring, the non-cooperative binding will

nonetheless cause some degree of charge neutralization on the phosphate backbone thereby allowing more of the redox probe to contact the gold surface. Thus, the lowered R_{CT} observed following exposure of the DNA to polylysine is likely due either to lowered negative charge density and condensation or due only to lowered negative charge density. Either of these effects would increase the accessibility of the gold surface to the redox probe.

The different results obtained following exposure of the dsDNA monolayer to spermine as compared to polylysine are likely due to the different properties of these two molecules. Spermine is known to cause DNA condensation (Wilson and Bloomfield, 1979). Spermine likely binds to the phosphate backbone (Vijayanathan *et al*., 2001), while different studies support binding in either the major (Feurstein *et al*., 1986) or minor (Schmid and Behr, 1991) groove. Interactions between spermine and DNA may also be sequence-dependent (Ruiz-Chica *et al*., 2001), although the study by Vijayanathan *et al*. in 2001 suggests that sequence plays little role in interactions between spermine and DNA. In contrast, interactions between polylysine and DNA cause different changes in the shape of DNA (Laemmli, 1975; Wagner *et al*., 1991) and are likely condensing DNA to a smaller extent than spermine (Trubetskoy *et al*., 1999). Polylysine binding is also believed to be largely entropy driven (Mascotti and Lohman, 1990) and may be cooperative depending on the ionic strength of the solution (Liu *et al*., 2001). The different sensitivities of this assay for spermine binding as compared to polylysine binding are likely due to the different modes of interaction between these two distinct molecules and DNA.

4.3 Binding of Actinomycin D to DNA Monolayers

Although actinomycin D is known to bind to dsDNA, there were no significant changes observed following exposure of a large concentration range of actinomycin D to the dsDNA monolayer. It is likely that binding occurred since the dsDNA sequence used to form the monolayer in these experiments contained the (dGdC)•(dGdC) sites that actinomycin is known to prefer (Chen *et al*., 1996). However, it is possible that the binding did not alter the structure of the DNA or otherwise alter the electronic or charge properties of the monolayer sufficiently to cause an observable signal. Unlike the polyamines, actinomycin D does not neutralize backbone phosphates and thus this indicates that it is possible that such neutralization may be important for observing a change in impedance of a DNA monolayer following binding of a small molecule. The studies described in Wang *et al*. 2003a and in Wang *et al.* 2003b both detected binding of actinomycin D to DNA by cyclic voltammetry

within the concentration range shown in figure 21. However, the cyclic voltammetry studies detected the interaction between actinomycin D and DNA through loss of actinomycin D redox activity upon binding to DNA and not through a change in impedance. The loss of redox activity of actinomycin D was believed to be because of sequestering of the redox-active phenoxazone ring between base pairs through intercalative binding (Wang *et al*., 2003a). One of the studies stressed that only electroactive ligands could be detected with this method (Wang *et al*., 2003b).

4.4 Binding of Methylated Bovine Serum Albumin to DNA Monolayers

The ΔR_{CT} observed following exposure of concentrations of 50 μg/mL me-BSA to the dsDNA monolayer is positive, indicating that the redox probe has less access to the gold surface. This is consistent with the me-BSA binding to the DNA and physically blocking the redox probe from contacting the gold surface, which would be expected if a large protein such as me-BSA were added to the monolayer. It is likely that me-BSA is binding to the DNA through interaction between positive charges on the protein and the negative charges on the phosphate backbone of the DNA. The increased R_{CT} would likely be due to steric effects restricting access of the redox probe to the gold surface since the ionic effects of me-BSA binding would serve to neutralize the phosphate backbone charges which, in isolation from any other effects, would likely lower the R_{CT} of the entire layer. When BSA was exposed to the monolayer, a significant signal was only observed at 1 mg/mL. However, the response observed following exposure of 1 mg/mL BSA to the DNA monolayer was less than half of the response observed following exposure of 500 μg/mL or 1 mg/mL me-BSA, indicating that even at 1 mg/mL, much less binding was occurring than with me-BSA. These results correlate well with observation that me-BSA, but not BSA, binds to DNA. The ΔR_{CT} that was observed between DNA and BSA could be due to deposition of BSA on to the monolayer through non-specific interactions or due to precipitation of the BSA on the electrode caused by high concentrations of the protein.

4.5 Binding of Antibodies to DNA Monolayers and to Plasmids

4.5.1 Jel 72

The low ΔR_{CT} observed following exposure of the dsDNA monolayer to Jel 72 may be due to the lack of poly(dG)•poly(dC), which Jel 72 is specific for, in the DNA sequences of the monolayer. This is true for both the 30mer and the 20mer. This result was expected given that the longest consecutive poly(dG)•poly(dC) sequence in the 20mer was only three nucleotides while the longest consecutive poly(dG)•poly(dC) sequence in the 30mer was only two nucleotides long. The band shift experiments described in section 3.7 showed binding of Jel 72 to pT463-I, which contains both poly(dG)•poly(dC) and poly(dTCC)•poly(dGGA) sequences (Lee *et al.*, 1989).

4.5.2 Jel 274

Given that Jel 274 is specific for the phosphate backbone of DNA and binds to random sequence DNA, it was unexpected that there was no significant ΔR_{CT} observed following exposure of the monolayer to Jel 274. It is possible that the monolayer was too densely packed to allow Jel 274 to bind to the phosphate backbone, but if this were the case it is surprising that dilution of the monolayer with butanethiol did not increase the ΔR_{CT} observed following exposure of the diluted monolayer to Jel 274. It is also possible that the solution of Jel 274 used in all experiments was denatured or otherwise inactive since there was no appreciable binding detected by gel electrophoresis band shift assays between this antibody, which lacks sequence specificity, and pT463-I. Finally, and perhaps most likely, the binding between Jel 274 and dsDNA may be too weak to show a significant signal on electrochemical measurements or to show retardation of the plasmid band in the electrophoresis experiments.

4.5.3 Hed 10

The low ΔR_{CT} values observed following exposure of the dsDNA monolayer to Hed 10 were expected given that Hed 10 is specific for ssDNA. Similarly, the large ΔR_{CT} values observed following exposure of the ssDNA monolayer to Hed 10 were also expected. As with the ΔR_{CT} values observed following exposure of the dsDNA monolayer to me-BSA, the ΔR_{CT}

values observed following exposure of the ssDNA monolayer to Hed 10 were large and positive, doubling the R_{CT} of the monolayer at the highest concentration. This likely indicates that the antibody is binding to the DNA, thereby restricting access of the redox probe to the gold surface, thus increasing the R_{CT} of the entire layer.

Although Hed 10 binds to DNA through ionic interactions with the phosphate backbone (Lee *et al*., 1982), which causes a lowering of the R_{CT} of the entire layer when polyamines bind to DNA, Hed 10 is a much larger molecule than either of the polyamines. Thus, similarly to binding of me-BSA to the DNA monolayer, there is likely a steric effect in addition to the charge neutralization effect occurring as a result of binding. It is likely that this steric effect is causing the positive ΔR_{CT} following exposure of the ssDNA monolayer to Hed 10. The steric effect is more significant than the charge neutralization effect or the overall ΔR_{CT} would be negative rather than positive. That Hed 10 showed significant and large signals with a ssDNA monolayer, but not dsDNA, demonstrates the potential for this technique to detect specific interactions between antibodies and DNA.

4.6 Summary

The experiments described in this thesis have shown much about the utility of an EIS-based assay for detecting and characterizing interactions between a DNA monolayer and a variety of different molecules. This work has established that binding of both proteins and small molecules to DNA monolayers can be detected with EIS. The signals generated by the former binding events are attributed to steric hindrance by the protein of the redox probe's access to the gold surface. Both non-specific and specific interactions between proteins and DNA were detected in experiments with me-BSA and with Hed-10, respectively. Signals resulting from binding of small molecules are attributed to conformational changes or charge neutralization taking place upon binding of small molecules to DNA. Experiments with actinomycin D show that not all conformational changes will manifest themselves by a change in impedance.

4.7 Future Directions

The next logical step with respect to detection of DNA-protein interactions by EIS is to define assays that can distinguish different modes of binding for both proteins and small molecules that interact with DNA. Establishing observable differences between various

binding modes in proteins will be another step towards making EIS a useful diagnostic tool, when used in combination with protein purification, for working with diseases that involve a DNA-binding protein, such as many autoimmune diseases. In order to better understand DNA-protein interactions, curve-fitting can be used on signals generated by well-understood DNA-protein interactions to separate the impact of changes in DNA conformation on the signal from the impact of steric inhibition of the redox probe's access to the gold surface.

Understanding the impacts of different changes in DNA conformation caused by different small molecules on EIS will lead to a further understanding of the electronic properties of DNA. This avenue of work will provide fruitful projects both in using the known effects of DNA-binding drugs on DNA conformation to ascertain what the EIS signal of those conformational changes are as well as probing the structural effects of new drugs using EIS as a tool. The individual aspects of impedance shown by a Randles or modified Randles circuit model applied to DNA can all change when the DNA undergoes a conformational change. Correlating changes in different aspects of the Randles or modified Randles circuit to known structural changes will deepen understanding of DNA structure in general and of the use of DNA on electrochemically sensitive monolayers in particular.

In summary, expanding on this work by better characterizing the effects of binding events between DNA and both proteins and small molecules and of conformational changes on the electronic properties of DNA will enhance understanding not only of the systems being studied themselves, but also of the effect of conformation on the electronic structure of DNA in general. Such work thus finds application both in relation to practical diagnostic applications and in relation to fundamental research on the physical properties of DNA.

5.0 Bibliography

Bain, C. D., H. A. Biebuyck, and G. M. **Whitesides.** 1989. Comparison of self-assembled monolayers on gold - coadsorption of thiols and disulfides. Langmuir. ***5***: 723-727.

Bard, A.J., and L.R. **Faulkner.** 2001. Electrochemical methods: fundamentals and applications. John Wiley & Sons Inc, New York

Barry, M. M. and Lee, J. S. 1993. Cloning and expression of an autoimmune DNA-binding single-chain Fv only the heavy-chain is required for binding. Mol. Immunol. **30**: 833-840.

Barry, M. M., C. D. Mol, W. F. Anderson, and J. S. **Lee.** 1994. Sequencing and modeling of anti-DNA immunoglobulin-Fv domains - comparison with crystal-structures. J. Biol. Chem. **269:**3623-3632.

Basu, H.S., R.H. Shafer, and L.J. **Marton.** 1987. A stopped-flow H-D exchange kinetic study of spermine-polynucleotide interactions. Nucleic Acids Res. **15**:5873-5886.

Biebuyck, H. A., and G. M. Whitesides. 1993. Interchange between monolayers on gold formed from unsymmetrical disulfides and solutions of thiols - Evidence for sulfur sulfur bond-cleavage by gold metal. Langmuir **9**:1766-1770.

Boodhoo, A., C. D. Mol, J. S. Lee, and W. F. Anderson. 1988. Crystallization of immunoglobulin Fab fragments specific for DNA. J. Biol. Chem. **263**:18578-18581.

Boon, E. M., J. E. Salas, and J. K. Barton. 2002. An electrical probe of protein-DNA interactions on DNA-modified surfaces. Nature Biotechnology **20**:282-286.

Braun, R. P., and J. S. Lee. 1986. Variations in duplex DNA conformation detected by the binding of monoclonal autoimmune antibodies. Nucleic Acids Res. **14**:5049-5065.

Carter, D. C., and J. X. Ho. 1994. Structure of serum albumin. Advances in protein chemistry **45**:153-203.

Chen, H. F., X. C. Liu, and D. J. Patel. 1996. DNA bending and unwinding associated with actinomycin D antibiotics bound to partially overlapping sites on DNA. J. Mol. Biol. **258**:457-47

Cygler, M., A. Boodhoo, J. S. Lee, and W. F. Anderson. 1987. Crystallization and structure determination of an autoimmune anti-poly(dT) immunoglobulin Fab fragment at 3.0 Å resolution. J. Biol. Chem. **262**:643-648.

Deng, H., V. A. Bloomfield, J. M. Benevides, and G. J. Thomas. 2000. Structural basis of polyamine-DNA recognition: spermidine and spermine interactions with genomic B-DNAs of different GC content probed by Raman spectroscopy. Nucleic Acids Res. **28:**3379-3385.

Eilat, D. 1982. Monoclonal autoantibodies: an approach to studying autoimmune disease. Mol. Immunol. **19**:943-955.

Feuerstein, B. G., N. Pattabiraman, and L. J. Marton. 1986. Spermine-DNA interactions: a theoretical study. Proc. Natl. Acad. Sci. USA **83:**5948-5952.

Feuerstein, B. G., N. Pattabiraman, and L. J. Marton. 1989. Molecular dynamics of spermine-DNA interactions: sequence specificity and DNA bending for a simple ligand. Nucleic Acids Res. **17**:6883-6892.

Figge, J., T. H. Rossing, and V. Fencl. 1991. The role of serum proteins in acid-base equilibria. J. Lab. Clin. Med. **117**:453-467.

Fraenkel-Conrat, H., and H. S. Olcott. 1945. Esterification of proteins with alcohols of low molecular weight. J. Biol. Chem. **161**:259-268.

Hahn, B. H. 2005. Systemic Lupus Erythematosus. In *Harrison's Principles of Internal Medicine*, 16th ed. (Edited by D. L. Kasper, E. Brauwald, A. S. Fauci, S. L. Hauser, D. L. Longo, and J.L. Jameson), McGraw-Hill, New York, pp. 1960-1967.

Hartwell, L.H., and M. B. Kastan. 1994. Cell cycle control and cancer. Science **266**:1821-1828

Haynes, B.F. and Facui, A.S. 2005. Introduction to the Immune System. In *Harrison's Principles of Internal Medicine*, 16th ed. (Edited by D. L. Kasper, E. Brauwald, A. S. Fauci, S. L. Hauser, D. L. Longo, and J.L. Jameson), McGraw-Hill, New York, pp. 1907-1930.

Herne, T. M., and M. J. Tarlov. 1997. Characterization of DNA probes immobilized on gold surfaces. J. Am. Chem. Soc. **119**:8916-8920.

Katayama, Y., M. Nakayama, H. Irie, K. Nakano, and M. Maeda. 1998. Bioaffinity sensor to anti-DNA antibodies using DNA modified Au electrode. Chem Lett. 1181-1182.

Koffler, D. 1974 Immunopathogenesis of systemic lupus erythematosus. Annu. Rev. Med. **25**:149-164.

Laemmli, U. K. 1975. Characterization of DNA condensates induced by poly(ethylene oxide) and polylysine. Proc. Natl. Acad. Sci. USA **72**:4288-4292.

Lafer, E. M., A. Moller, A. Nordheim, B. D. Stollar, and A. Rich, 1981. Antibodies specific for left-handed Z-DNA. Proc. Natl. Acad. Sci. USA. **78**:3546-3550.

Latt, S.A., and H.A. Sober. 1967. Protein-nucleic acid interactions. II. Oligopeptide-polyribonucleotide binding studies. Biochemistry. **6**:3293-3306

Lee, J. S., J. R. Lewis, A. R. Morgan, T. R. Mosmann, and B. Singh. 1981. Monoclonal-antibodies showing sequence specificity in their interaction with single-stranded DNAs. Nucleic Acids Res. **9**:1707-1721.

Lee, J. S., D. F. Dombroski, and T. R. Mosmann, 1982. Specificity of autoimmune monoclonal Fab fragments binding to single-stranded deoxyribonucleic-acid. Biochemistry **21**:4940-4945.

Lee, J. S., M. L. Woodsworth, and L. J. P. Latimer. 1984. Monoclonal-antibodies specific for poly(dG)•poly(dC) and poly(dG)•poly(dm^{5}C). Biochemistry **23**:3277-3281.

Lee, J. S., G. D. Burkholder, L. J. P. Latimer, B. L. Haug, and R. P. Braun, 1987. A monoclonal antibody to triplex DNA binds eukaryotic chromosomes. Nucleic Acids Res. **15**:1047-106.

Lee, J.S., L.J.P. Latimer, B.L. Haug, D.E. Pulleyblank, D.M. Skinner, and G.D. Burkholder. 1989. Triplex DNA in plasmids and chromosomes. Gene **82**:191-199.

Li, C. Z., Y. T. Long, H. B. Kraatz, and J. S. Lee. 2003. Electrochemical investigations of M-DNA self-assembled monolayers on gold electrodes. J. Phys. Chem. B. **107**:2291-2296

Lipsky, P.E., and B. Diamond, 2005. Autoimmunity and autoimmune diseases. In *Harrison's Principles of Internal Medicine*, 16th ed. (Edited by D. L. Kasper, E. Brauwald, A. S. Fauci, S. L. Hauser, D. L. Longo, and J.L. Jameson), McGraw-Hill, New York, pp. 1956-1960

Liu, G., M. Molas, G. A. Grossmann, M. Pasumarthy, J. C. Perales, M. J. Cooper, and R. W. Hanson. 2001. Biological properties of poly-L-lysine-DNA complexes generated by cooperative binding of the polycations. J. Biol. Chem. **276**:34379-34387.

Long, Y. T., C. Z. Li, T. C. Sutherland, M. Chahma, J. S. Lee, and H. B. Kraatz. 2003. A comparison of electron-transfer rates of ferrocenoyl-linked DNA. J. Am. Chem. Soc. **125**:8724-8725.

Luscombe, N.M., R.A. Laskowski, and J.M. Thorton. 2001. Amino acid-base interactions: a three-dimensional analysis of protein-DNA interactions at an atomic level. Nucleic Acids Res. **29**:2860-2874.

Marmur, J., and P. Doty. 1962. Determination of base composition of deoxyribonucleic acids from its thermal denaturation temperature. J. Mol. Biol. **5**:109-118.

Masamune, Y. 1964. Fractionation of vegetative pool deoxyribonucleic acid of bacteriophage T2 by methylated bovine serum albumin column. J. Bioch. **55**:116-121.

Mascotti, D. P., and T. M. Lohman. 1990. Thermodynamic extent of counterion release upon binding oligolysines to single-stranded nucleic-acids. Proc. Natl. Acad. Sci. USA **87**:3142-3146.

McCall, M., T. Brown, and O. Kennard. 1985. The crystal-structure of d(G-G-G-G-C-C-C-C) - a model for poly(dG)•poly(dC). J. Mol. Biol. **183**:385-396.

Minyat, E., V. Ivanov, A. Kritzyn, L. Minchenkova, and A. Schyolkina. 1978. Spermine and spermidine-induced B to A transition of DNA in solution. J. Mol. Biol. **128**:397-409.

Mol, C. D., A. K. S. Muir, J. S. Lee, and W. F. Anderson. 1994. Structure of an immunoglobulin Fab fragment specific for poly(dG)•poly(dC). J. Biol. Chem. **269**:3605-3614.

Moller, A., J. E. Gabriels, E. M. Lafer, A. Nordheim, A. Rich, and B. D. Stollar. 1982. Monoclonal antibodies recognize different parts of Z-DNA. J. Biol. Chem. **257**:2081-2085.

Nuzzo, R. G., and D. L. Allara, 1983. Adsorption of bifunctional organic disulfides on gold surfaces. J. Am. Chem. Soc.**105**:4481-4483.

Roeder, R.G. 2005. Transcriptional regulation and the role of diverse coactivators in animal cells. FEBS Lett. **579**:909-915

Ruiz-Chica, J., M. A. Medina, F. Sanchez-Jimenez, and F. J. Ramirez. 2001. Fourier transform Raman study of the structural specificities on the interaction between DNA and biogenic polyamines. Biophys. J. **80**:443-454.

Schmid, N., and J. P. Behr. 1991. Location of spermine and other polyamines on DNA as revealed by photoaffinity cleavage with polyaminobenzenediazonium salts. Biochemistry **30**:4357-4361.

Shoenfeld, Y., J. Rauch, H. Massicotte, S. K., Datta, J. Andreschwartz, B. D. Stollar, and R. S. Schwartz. 1983. Polyspecificity of monoclonal lupus autoantibodies produced by human-human hybridomas. New Eng. J. Med. **308**:414-420.

Sinden, R.R. 1994. DNA Structure and function. Academic Press, San Diego

Sober, H.A., S.F. Schlossman, A. Yaron, S.A. Latt, and G.W. Rushizky. 1966. Protein-nucleic acid interaction. I. Nuclease-resistant polylysine-ribonucleic acid complexes. Biochemistry **5**:3608-3616

Steel, A. B., T. M. Herne, and M. J. Tarlov. 1998. Electrochemical quantitation of DNA immobilized on gold. Anal. Chem. **70**:4670-4677.

Steel, A. B., R. L. Levicky, T. M. Herne, and M. J. Tarlov. 2000. Immobilization of nucleic acids at solid surfaces: effect of oligonucleotide length on layer assembly. Biophys J. **79**:975-981.

Swanson, P. C., C. Ackroyd, and G. D. Glick. 1996. Ligand recognition by anti-DNA autoantibodies. Affinity, specificity, and mode of binding. Biochemistry **35**:1624-1633.

Stollar, B.D. 1994. Molecular analysis of anti-DNA antibodies. FASEB J. **8**:337-342.

Swanson, P.C., C. Ackroyd, and G.D. Glick. 1996. Ligand recognition by anti-DNA antibodies. Affinity, specificity, and mode of binding. Biochemistry **35**:1624-1633.

Tabor, C. W., and H. Tabor, 1984. Polyamines. Ann. Rev. Bioch. **53**:749-790.

Tanha, J., and J. S. Lee. 1997. Thermodynamic analysis of monoclonal antibody binding to duplex DNA. Nucleic Acids Res. **25**:1442-1449.

Trubetskoy, V. S., P. M. Slattum, J. E. Hagstrom, J. A. Wolff, and V. G. Budker, 1999. Quantitative assessment of DNA condensation. Anal. Bioch. **267**:309-313.

Truong, K. D., and P. A. Rowntree, 1995. Kinetics of the formation of butanethiol monolayers on gold substrates, as studied by infrared spectroscopy. Progress in Surface Science **50**:207-216.

Tsao, B.P., F.M. Ebling, C. Roman N. Panosian-Sahakian, K. Calame, B.H. Hahn. 1990. Structural characteristics of the variable regions of immunoglobulin genes encoding a pathogenic autoantibody in murine lupus. J Clin Invest. **85**: 530–540.

van den Berg, W. B., L. B. A. van de Putte, W. A. Zwarts, and L. A. B. Joosten. 1984. Electrical charge of the antigen determines intraarticular antigen handling and chronicity of arthritis in mice. J. Clin. Invest. **74**:1850-1859.

Vijayanathan, V., T. Thomas, A. Shirahata, and T. J. Thomas. 2001. DNA condensation by polyamines: a laser light scattering study of structural effects. Biochemistry. **40**:13644-13651.

Wadkins, R. M., E. A. JaresErijman, R. Klement, A. Rudiger, and T. M. Jovin. 1996. Actinomycin D binding to single-stranded DNA: sequence specificity and hemi-intercalation model from fluorescence and H-1 NMR spectroscopy. J. Mol. Biol. **262**:53-68.

Wagner, E., M. Cotten, R. Foisner, and M. L. Birnstiel. 1991. Transferrin polycation DNA complexes - the effect of polycations on the structure of the complex and DNA delivery to cells. Proc. Natl. Acad. Sci. USA **88**:4255-4259.

Wang, S., T. Z. Peng, and C. F. Yang. 2003. Investigation of the interaction of DNA and actinomycin D by cyclic voltammetry. J. Electroanal. Chem. **54**:87-92. (a)

Wang, S., Peng, T. and Yang, C. F. 2003. Investigation on the interaction of DNA and electroactive ligands using a rapid electrochemical method. J. Biochem. Biophys. Methods **55**:191-204. (b)

Watson, J. D., and F. H. C. Crick. 1953. Molecular structure of nucleic acids - a structure for deoxyribose nucleic acid. Nature **171**:737-738.

Wilson, R. W., and V. A. Bloomfield. 1979. Counterion-induced condensation of deoxyribonucleic acid. Biochemistry **18**:2192-2196.